Nuclear Engineering and Design 427 (2024) 113430

Contents lists available at ScienceDirect

Nuclear Engineering and Design

journal homepage: www.elsevier.com/locate/nucengdes

# Investigation of the PCMI failure of pre-hydrided Zy-4 cladding during Reactivity Initiated Accidents with ALCYONE and OFFBEAT fuel performance codes

Matthieu Reymond [a,b,*], Jérôme Sercombe [b], Alessandro Scolaro [a]

[a] Ecole Polytechnique Fédérale de Lausanne (EPFL) - Laboratory for Reactor Physics and Systems Behaviour, 1015 Lausanne, Switzerland
[b] CEA, DES, IRESNE, DEC, 13018 Saint-Paul-Lez-Durance, France

## ARTICLE INFO

Dataset link: https://gitlab.com/foam-for-nuclear/offbeat

*Keywords:*
Reactivity Initiated Accident
High Burnup Experiments in Reactivity Initiated Accident (HERA)
Hydrided cladding
PCMI failure
ALCYONE
OFFBEAT

## ABSTRACT

This paper presents simulations of Reactivity Initiated Accident on PWR fuel rods performed with two fuel performance codes: ALCYONE and OFFBEAT. These simulations were carried out in the framework of the first phase of the High-Burnup Experiments of Reactivity Initiated Accident (HERA) project of the Nuclear Energy Agency (NEA). The focus of this project is the hydride assisted cladding failure during the Pellet-Clad Mechanical Interaction phase of the transient. In the simulations performed with ALCYONE and OFFBEAT, cladding mechanical behavior is simulated with an anisotropic viscoplastic law dependent on temperature, strain rate and hydrogen content. Clad failure is predicted with a hoop strain criterion, taking into account the impact of strain-rate, temperature, hydrogen content and hydride rim thickness and the ductility recovery that occurs at moderate or elevated temperature due to the dissolution of hydrides. The validation of the proposed failure criterion is based on 2D-(r$\theta$) simulations performed with ALCYONE that allows to explicitly model cracking of the hydride rim at the cladding periphery and the resulting strain localization in the remaining sound clad ligament beneath it. The results of the simulations performed with ALCYONE 1.5D or OFFBEAT 2D-(rz) are in good agreement with the ALCYONE 2D-(r$\theta$) results, thus indicating that the proposed failure criterion is able to account for the detrimental effect of the hydride rim in ALCYONE 1.5D or OFFBEAT simulations. Finally, the calculated enthalpies at failure as a function of the hydrogen content/hydride rim thickness are shown to be consistent with previous experimental results obtained in the NSRR test facility.

## 1. Introduction

The number of experimental programs dedicated to RIA has increased in the past years. Among them, the Cabri International Program (NEA CIP, 2024), performed at the CABRI research reactor (France), aims at investigating the Departure from Nucleate Boiling (DNB) phase of the transient and the potential post-DNB failure. The High-burnup Experiments in Reactivity Initiated Accident (HERA) Joint Experimental Program (NEA HERA, 2024) has been launched in 2023 as part of the Nuclear Energy Agency (NEA) Framework for Irradiation Experiments (NEA FIDES, 2024). The first phase of the project is focused on the Pellet-Cladding Mechanical Interaction (PCMI) phase of a RIA transient and consists in 4 integral experiments performed at the Nuclear Safety Research Reactor (NSSR, Japan) and at the Transient Reactor Test Facility (TREAT, USA). Simultaneously, the HERA Joint Experimental Program coordinated a Modeling & Simulation (M&S) exercise to evaluate the design and to interpret the experiments. The first phase of this M&S exercise that is the subject of the present work consisted in conducting blind simulations of 12 experiments based on the 4 real HERA experiments. This exercise brought together 23 organizations and 14 fuel performance codes (Folsom et al., 2023; Seo et al.). The goal of these simulations is the study of the PCMI phase that occurs at the beginning of the pulse. It is commonly accepted that failure by PCMI depends heavily on the degradation of the mechanical properties of the cladding due to hydrogen pick-up and precipitation into solid hydrides, on the kinetics of the pulse and on the total energy injected in the fuel rod (Papin et al., 2007; Tomiyasu et al., 2007; Fuketa et al., 1997; NEA - Working Group on Fuel Satefy, 2022a; Fuketa et al., 2006). The investigation of the impact of pulse kinetics is achieved by testing the same fuel rods in two research reactors: the NSRR (fast pulses, Full Width Half Maximum 7.5 ms) and TREAT (slow pulses, Full Width Half Maximum between 50 and 300 ms) facilities. The impact of hydride embrittlement is investigated by considering

* Corresponding author at: Ecole Polytechnique Fédérale de Lausanne (EPFL) - Laboratory for Reactor Physics and Systems Behaviour, 1015 Lausanne, Switzerland.
*E-mail address:* matthieu.reymond@epfl.ch (M. Reymond).

https://doi.org/10.1016/j.nucengdes.2024.113430
Received 16 April 2024; Received in revised form 26 June 2024; Accepted 27 June 2024
Available online 10 July 2024

**Nomenclature**

| | |
|---|---|
| $\varepsilon_{\theta\theta}^{f}$ | Hoop plastic strain at failure |
| $C_{pp}$ | Hydrogen concentration in solid precipitates |
| $C_{ss}$ | Hydrogen concentration in solid solution |
| $C_{tot}$ | Hydrogen concentration |
| $f_2$ | Cladding ductility reduction factor related to hydrogen-induced embrittlement |
| $S_0$ | $S_{rim}$ value at room temperature |
| $S_{recovery}$ | Recovery factor applied to $S_0$ to take into account the ductility recovery at moderate or high temperatures |
| $S_{rim}$ | Cladding ductility reduction factor related to the hydride rim induced embrittlement |
| $t_{rim}$ | Hydride rim thickness at room temperature |
| $TSS$ | Terminal Solubility Limit of hydrogen in Zircaloy-4 |
| HERA | High-burnup Experiments in Reactivity Initiated Accident |
| NEA | Nuclear Energy Agency |
| NSRR | Nuclear Safety Research Reactor |
| RIA | Reactivity Initiated Accident |
| TREAT | Transient Reactor Test Facility |

three different hydride rim thicknesses (40, 80, 140 μm). Finally, the magnitude of the pulses is adjusted to target three different peak radial average enthalpy increase of 550, 650 and 750 J/g.

The Laboratory for Reactor Physics and Systems Behaviour of the Ecole Polytechnique Fédérale de Lausanne (EPFL, Switzerland) and the Commissariat à l'Energie Atomique et aux Energies Alternatives (CEA, France) participated to the M&S exercise in close collaboration with their respective fuel performances codes: OFFBEAT (EPFL) and ALCYONE (CEA). This paper presents the recent developments made in OFFBEAT for the simulation of RIA transients, using as a reference ALCYONE for comparison and validation purposes. At the same time, this paper presents the methodology and underlying models for clad failure predictions used in OFFBEAT and ALCYONE in the framework of the HERA M&S exercise.

OFFBEAT is an open-source multi-dimensional fuel performance code (Scolaro et al., 2020; Scolaro, 2021) based on the Finite Volume Method library OpenFOAM, developed since 2017 at the EPFL, in collaboration with the Paul Scherrer Institute. Until recently, main applications, developments and validation efforts have focused mostly on base irradiation conditions (Scolaro et al., 2022a). Recent and ongoing work related to PWR applications focuses on providing off-normal or accidental related capabilities to OFFBEAT (Brunetto et al., 2023; Reymond et al., 2024; Zullo et al., 2024).

ALCYONE is a multidimensional finite element fuel performance code, co-developed within the PLEIADES software environment by the CEA, EDF and Framatome, and dedicated to the simulation of PWR fuel rod behavior in normal or off-normal conditions (Introïni et al., 2024; D'Ambrosi et al., 2023; Germain et al., 2022; Guénot-Delahaie et al., 2018; Sercombe et al., 2020). ALCYONE is a well validated code for PWR-$UO_2$ fuel rods tested in a stagnant water coolant initially at room temperature and atmospheric pressure as in the NSRR and TREAT experimental facilities. The parameters of the boiling curve used to describe the clad-to-coolant heat exchanges have recently been recalibrated for NSRR conditions (Guénot-Delahaie et al., 2022), making ALCYONE a reference code for the experiments considered in this study. Moreover, ALCYONE possesses a specific 2D-(r$\theta$) scheme to predict failure by PCMI for hydrided cladding, taking into account the shape and thickness of the hydride rim or lenticular hydride blister (Sercombe et al., 2016).

In this paper, we first present the implementation, in both OFFBEAT and ALCYONE, of a dedicated mechanical model for Zircaloy-4 cladding that takes into account the local hydrogen content of the cladding and its distribution in solid solution or in solid precipitates. We then present a strain failure criterion dependent on temperature, hydrogen content, strain rate and rim thickness to assess clad failure in 1.5D (ALCYONE) or 2D-(rz) (OFFBEAT) simulations. This failure criterion is based on the model proposed by Jernkvist et al. (2004) and is extended to account for the thickness of the hydride rim and its deleterious effect on clad mechanical properties. In the third part of this paper, HERA transients and specimens are presented as well as general modeling hypotheses. The results of 1.5D or 2D-(rz) simulations are then detailed and the failure times and corresponding enthalpies at failure are compared to the results of the 2D-(r$\theta$) simulations performed with ALCYONE. As the latter scheme explicitly takes into account the thickness of the rim, it is considered as a reference and is used to validate the proposed clad failure criterion. Finally, these results are compared to experimental data from previous integral tests performed in the NSRR facility.

## 2. Modeling of hydrided cladding

### 2.1. Mechanical model for hydrided and unirradiated Zircaloy-4 cladding

The loading conditions during a RIA can lead to high cladding temperatures, stresses and strain rates. We thus implemented in OFFBEAT and ALCYONE the anisotropic model of M. Le Saux et al. for unirradiated and hydrided Zy-4 cladding tubes (Le Saux et al., 2015). It describes the anisotropic mechanical behavior of hydrided Zy-4 (up to an hydrogen content of 1200 wt.ppm) in relevant temperature (from 25 to 1100 °C) and strain rate ranges (from $3\times10^{-4}$ up to 5 /s). It consists in an unified viscoplastic formulation with no stress threshold between the elastic and viscoplastic regimes. The plastic anisotropy induced by the crystallographic texture of stress relieved Zy-4 is described by Hill's quadratic criterion:

$$\sigma_{\mathrm{eq}}^{\mathrm{H}} = \sqrt{\underline{\sigma} : \underline{\underline{H}} : \underline{\sigma}} \tag{1}$$

with $\sigma_{\mathrm{eq}}^{\mathrm{H}}$ the equivalent stress linked to the stress tensor $\underline{\sigma}$ via Hill's tensor $\underline{\underline{H}}$. In a cylindrical coordinate system (r, $\theta$,z), we can express the equivalent stress as given in Box I,

where $H_{rr}$, $H_{\theta\theta}$, $H_{zz}$, $H_{r\theta}$, $H_{rz}$ and $H_{\theta z}$ are Hill's parameters. The viscoplastic strain rate $\dot{p}$ is linked to the stress tensor $\underline{\sigma}$ and to the cumulated equivalent viscoplastic strain $p$ as follows:

$$\dot{p} = \left( \frac{\sigma_{eq}^{H}(\underline{\sigma}, T)}{K(T, C_{ss}, C_{pp}) \times L(p, T, C_{pp})} \right)^{1/m(T)} \tag{3}$$

where $T$ is the temperature in Kelvin, $\sigma_{eq}^{H}$ is the equivalent stress in MPa, $m$ is the strain sensitivity exponent (unitless), $K$ is the strength coefficient in MPa and $L$ is the strain hardening coefficient (unitless). The strength coefficients depends on the hydrogen concentration (wt.ppm) in solid solution $C_{ss}$ and in solid precipitates $C_{pp}$ while the strain hardening coefficient is only a function of $C_{pp}$. The strength coefficient of the material increases linearly with the hydride concentration. The strain hardening coefficient is a non linear function of the hydride concentration. At ambient temperature for example, a higher hydride concentration will lead to slightly more hardening if the equivalent viscoplastic strain is below 0.02, as reported by Le Saux et al. (2009). The parameters of the model are given in Table 1.

The cladding tubes of the Phase 1 of the HERA project are artificially hydrided prior to the transients to mimic the hydride structure typically observed in a high burnup LWR Zy-4 rod after irradiation. During the PCMI phase of the transient, which is the focus of this work, the cladding temperature increases and dissolution of hydrides could potentially occur. Dissolution is a fast mechanism that is often considered instantaneous (Courty et al., 2014). Indeed, simulations of the

$$\sigma_{\mathrm{eq}}^{\mathrm{H}} = \sqrt{H_{rr}\left(\sigma_{\theta\theta}-\sigma_{zz}\right)^2 + H_{\theta\theta}\left(\sigma_{zz}-\sigma_{rr}\right)^2 + H_{zz}\left(\sigma_{rr}-\sigma_{\theta\theta}\right)^2 + 2H_{r\theta}\sigma_{r\theta}^2 + 2H_{rz}\sigma_{rz}^2 + 2H_{\theta z}\sigma_{\theta z}^2} \quad (2)$$

**Box I.**

**Table 1**
Cladding mechanical model parameters, from Le Saux et al. (2015). T is the temperature in Kelvin, $C_{ss}$ and $C_{pp}$ are the hydrogen concentrations in solid solution and in solid precipitates, in wt.ppm.

| |
|---|
| Strain rate sensitivity exponent m:<br>$m = \frac{1}{77.68M_T + 4.11(1-M_T)}$<br>where $M_T = \frac{1}{1+\exp(10.2(T/692-1))}$ |
| Strain hardening coefficient L:<br>$L = (p+1\times10^{-4})^{n_0}\exp(-\alpha_n p) + (1-\exp(-\alpha_n p))$<br>with $n_0 = (1+1.45\times10^{-4}C_{pp})\left[4.86\times10^{-2}N_{0T} + 2.35\times10^{-2}(1-N_{0T})\right]$<br>where $N_{0T} = \frac{1}{1+\exp\left(12\left(\frac{T}{(810-9.19\times10^{-2}C_{pp})}-1\right)\right)}$<br>and $\alpha_n = (53.16+1.27\times10^{-2}C_{pp})(1+\exp(11.1(T/738-1)))$ |
| Strength coefficient K:<br>$K = \left[1-1.175\times10^{-4}C_{ss} + (6.15\times10^{-5}-4.38\times10^{-8}T)C_{pp}\right]$<br>$\left[(1.409\times10^{9}-8.952\times10^{5}T)K_T + 4.05\times10^{7}(1-K_T)\right]$<br>where $K_T = \frac{1}{1+\exp(1.77(T/1007-1))}$ |
| Plastic anisotropy coefficients:<br>$H_{rr} = \frac{0.485+9.5\times10^{-2}}{1+\exp(12(T/740-1))}$<br>$H_{\theta\theta} = 1-H_{rr}$<br>$H_{zz} = \frac{0.52+(-0.23+4\times10^{-4}T)}{1+\exp(12(T/550-1))}$<br>$H_{r\theta} = H_{rz} = H_{\theta z} = 1.5$ |

hydrogen distribution (dissolved or precipitated) during a NSRR pulse, by considering an instantaneous dissolution mechanism or by using the kinetics term measured by Lacroix et al. (2018), have shown negligible differences. For this reason, in this study, we consider hydride nucleation, growth and dissolution to be instantaneous. The distribution of hydrogen between the solid solution and the hydride precipitates is estimated from the terminal solubility limit of hydrogen in Zircaloy-4. The correlation proposed by Kearns (Kearns, 1967) is considered in this work:

$$TSS = 99000\exp(-34523/\mathrm{RT})\ \text{[wt.ppm]} \quad (4)$$

where R is the gas constant in J/mol/K and $T$ the temperature in Kelvin. For a given hydrogen concentration $C_{tot}$, the distribution between the solid solution and the solid precipitates is given as a function of the temperature $T$ in Kelvin by:

$$\begin{aligned} C_{ss}(T) &= \min(C_{tot}, TSS(T))\ \text{[wt.ppm]} \\ C_{pp}(T) &= C_{tot} - C_{ss}(T)\ \text{[wt.ppm]} \end{aligned} \quad (5)$$

Hydrogen diffusion in the cladding is not considered and the concentration of hydrogen in a given element or cell is constant during the simulation and corresponds to its initial value.

### 2.2. Clad failure criterion

To assess clad failure, we consider the strain criterion of Jernkvist et al. (2004). It defines a hoop plastic strain threshold at which failure occurs, taking into account the impact of temperature, strain rate, excess hydrogen content, irradiation damage and external zirconia spalling. Cladding is considered as failed when the radial average hoop plastic strain at a given axial location in a fuel rod exceeds a critical value $\varepsilon_{\theta\theta}^{f}$ given by:

$$\varepsilon_{\theta\theta}^{f} = \frac{3\cdot S_{spalling}\cdot\varepsilon_{\theta\theta}^{0}\cdot f_1\cdot f_2\cdot f_3}{f_1\cdot f_2 + f_1\cdot f_3 + f_2\cdot f_3} \quad (6)$$

where $\varepsilon_{\theta\theta}^{0}$ is the hoop plastic strain at failure of as-fabricated cladding with negligible hydrogen content and at low strain rate, given as a function of temperature and relevant to the geometry and loading under RIA (i.e., biaxial loading $\frac{\sigma_{zz}}{\sigma_{\theta\theta}} = 1$). The model then considers 3 different reduction factors $f_1$, $f_2$, $f_3$ accounting for the impact of elevated strain rates (max. 1 $s^{-1}$), hydrogen induced embrittlement (max. 750 wt.ppm) and irradiation damage, respectively. The expressions of $\varepsilon_{\theta\theta}^{0}$, $f_1$ and $f_2$ are given Table 2. In this study, as unirradiated cladding is considered, the $f_3$ factor is equal to one. $S_{spalling}$ is a fourth ductility reduction factor for cladding tubes with spalled zirconia, that is also not relevant here, thus it is also equal to one. The parameters were established from out-of-pile tests conducted on uniformly hydrided or irradiated samples. Therefore, the impact of a hydrogen concentration gradient and of a hydride rim are not considered. This is an important limitation of the model for its application to HERA tests since the presence of a hydride rim is known to decrease the mechanical properties of the cladding tubes as it is a preferential site for crack initiation (Chung and Kassner, 1998; Tomiyasu et al., 2007). Note that for the interpretation of out-of-pile experiments such as burst tests, the hoop plastic strain at failure of as-fabricated cladding must be corrected to account for the stress-biaxiality ratio of these experiments that differs from the one relevant for RIA conditions. For normal burst tests $\left(\frac{\sigma_{zz}}{\sigma_{\theta\theta}} = 0.5\right)$, that are used in the next section, the hoop plastic strain at failure $\varepsilon_{\theta\theta}^{0}$ must be divided by the following factor:

$$C_{R1} = \frac{\underline{\varepsilon}_{te}(\sigma_{zz}/\sigma_{\theta\theta}=1)}{\underline{\varepsilon}_{te}(\sigma_{zz}/\sigma_{\theta\theta}=0.5)} = 0.456 \quad (7)$$

With $\underline{\varepsilon}_{te}$ the average hoop total elongation evaluated from the experimental data presented by Andersson and Wilson (1979) and Maki and Ooyama (1975).

#### 2.2.1. Hydride rim thickness dependency

We hereafter propose an extension of the failure criterion of Jernkvist to account for the rim thickness and its impact on the strain at failure of cladding tubes. This is achieved by introducing the $S_{rim}$ reduction factor instead of $S_{spalling}$, as zirconia spalling is not relevant for the HERA tests (no oxide layer is present at the outer wall of the cladding tubes). This extension is based on the work of Nagase and Fuketa (2005), who performed a series of burst tests on hydrogen-charged low-tin Zircaloy-4 cladding tubes.

Briefly, the samples were hydrogenated in a mixture of hydrogen and argon at 620 K during various times, resulting in samples with different hydrogen average contents, presenting hydride rims of thicknesses between 100 and 170 μm. Burst tests were conducted at 293 or 623 K with a pressurization rate of 0.002, 0.2 or 2 GPa/s (corresponding to strain rates of $5\times10^{-4}$, 0.05 and 0.5 $s^{-1}$). At room temperature, the authors reported a decrease of the residual hoop strain with increasing hydrogen concentration and pressurization rate, with the former being the main parameter degrading the mechanical properties of the samples. At an average hydrogen content of around 300 wt.ppm, the presence of a hydride rim slightly decreased the residual strain, from 1.33% without a rim and at a loading rate of 2 GPa/s to 0.5%. At 623 K, the impact of the hydride rim was more significant: at around 600 wt.ppm, the residual hoop strain was 12% without a rim while it was reported to be as low as 0.5% with a rim structure. These results indicate that not only the total hydrogen content, temperature or strain rate played a role on the mechanical

**Table 2**
Parameters of the failure criterion proposed by Jernkvist et al. (2004).

| |
|---|
| Hoop plastic strain at failure for as fabricated cladding tubes (equi-biaxial conditions) : $\varepsilon^0_{\theta\theta}(T) = 2.82 + 1.22 \times 10^{-2}\mathrm{T}$ [%] |
| $f_1$ ductility reduction factor (effect of strain rate): $f_1(\dot{\varepsilon}) = \begin{cases} 0.046 - 0.31 \times \log_{10}\dot{\varepsilon} & \text{if } \dot{\varepsilon} \leq 1\,\mathrm{s}^{-1} \\ 0.046 & \text{if } \dot{\varepsilon} > 1\,\mathrm{s}^{-1} \end{cases}$ |
| $f_2$ ductility reduction factor (effect of hydrogen content): $f_2(C_{pp}, T, \dot{\varepsilon}) = 0.01 + 0.99 \times \exp(-\gamma(T, \dot{\varepsilon})C_{pp})$ With $C_{pp}$ the hydride concentration in wt.ppm, T the temperature in K and $\dot{\varepsilon}$ the strain rate in $\mathrm{s}^{-1}$. |
| The hydride concentration is given by: $C_{pp}(T) = \max(0, (\mathrm{C_{tot}} - TSS(T)))$ With T the temperature in K, $C_{tot}$ the total hydrogen content in wt.ppm and TSS the terminal solubility limit in wt.ppm: $\mathrm{TSS} = 99000\exp(-34523/\mathrm{RT})$ With T the temperature in K and R the gas constant in J/mol/K. |
| The $\gamma$ function is given by: $\gamma(T, \dot{\varepsilon}) = 6.52 \cdot 10^{-4} + 2.21 \cdot 10^{-3}(6 + \log_{10}\dot{\varepsilon})\left(1 - \tanh\left(\frac{T - T_{transition}}{wf}\right)\right)$ with $T_{transition}$ equal to 298 K and $wf$ equal to 8.5. |

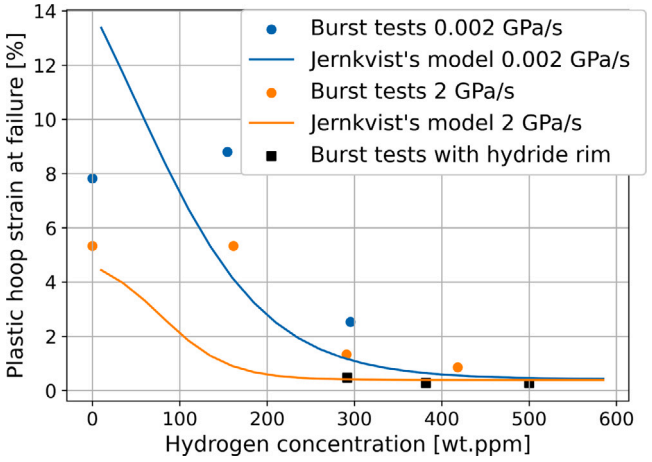


**Fig. 1.** Plastic hoop strain at failure reported by Nagase and Fuketa (2005) for the burst tests conducted at room temperature. The lines correspond to the to predicted failure strains according to the failure criterion proposed by Jernkvist et al. (2004).

properties of the samples, but the presence of a dense hydride rim also significantly altered the mechanical properties in these conditions.

As one can see in Fig. 1, the criterion proposed by Jernkvist et al. works reasonably well for the tests at low temperatures. It is consistent with the fact that at room temperature, the presence of a rim structure does not seem to significantly impact the mechanical behavior of the cladding tubes.

Conversely, at 623 K, the failure criterion proposed by Jernkvist et al. does not fit with the measurements of Nagase and Fuketa (Fig. 2, left), in particular when the hydrogen concentration exceeds 500 wppm.

Based on these considerations, we propose the introduction of the $S_{rim}$ reduction factor to take into account the impact of the rim thickness on the mechanical properties of Zircaloy-4. The $S_{rim}$ reduction factor is given by:

$$S_{rim} = S_0(t_{rim}) \times S_{recovery}(T_{rim}, C_{ss,rim}) \tag{8}$$

$S_{rim}$ is the product of $S_0$, a function of the hydride rim thickness at room temperature, $t_{rim}$ given in μm, and of $S_{recovery}$, a function of $T_{rim}$, the temperature in K at the rim depth, and of the hydrogen concentration in solid solution in the rim ($C_{ss,rim}$). $S_0$ is a reduction factor that rapidly decreases from 1 to a minimal value of 0.05 when the hydrogen concentration increases from 200 to 500 wt.ppm, to which corresponds a rim thickness of 40 to 70 μm, in agreement with the results of Nagase and Fuketa (2005). It is given by:

$$S_0(t_{rim}) = \min\left(\max\left(0.05, 1 - \frac{(1 - 0.05)}{70} \times (t_{rim} - 50)\right), 1\right) \tag{9}$$

This reduction factor accounts for the detrimental effect of a hydride rim on the hoop plastic strain at failure at room temperature. At moderated or elevated temperatures, partial or total dissolution of the hydrides is expected. Ductility recovery is thus introduced in the strain criterion with a recovery factor, noted $S_{recovery}$ that reads as follows:

$$S_{recovery}(T_{rim}) = S_0 + \frac{C_{ss,rim}}{C_{tot,rim}} \times (1 - S_0) \tag{10}$$

As the brittle hydride rim is expected to fail early when mechanically loaded, thus creating a crack that reduces the strength and ductility of the cladding, the recovery factor considers $T_{rim}$ the temperature at the crack tip in Kelvin and $C_{ss,rim}$ the dissolved hydrogen in the rim, obtained with Eq. (5). For transient simulations, the temperature at the crack tip (i.e., the temperature at the depth of the rim) is lower than the average temperature of the cladding. The recovery of ductility resulting from hydrides dissolution is assumed to be proportional to the fraction of dissolved hydrides. Thus, if the temperature reached during the transient is high enough to completely dissolve the hydride rim, $C_{ss,rim} = C_{tot,rim}$ and $S_{rim} = 1$ and the original model of Jernkvist et al. (2004) is recovered. The predicted failure strain as a function of hydrogen content with this reduction factor when applied to the burst tests of Nagase and Fuketa (2005) is plotted in Fig. 2 (right graph). It predicts more accurately the behavior of the samples that presented a rim at their outer periphery.

To relate the hydride rim thickness (in μm) to the average hydrogen content (in wt.ppm) of the samples used by Nagase and Fuketa (2005), the following relation was derived from the measurements of the authors:

$$t_{rim} = 86.40 \times \ln(\mathrm{AverageHydrogenContent}) - 415.63\ [\mu m] \tag{11}$$

This relationship is specific to the hydrogenating protocol used by Nagase and Fuketa (2005), which is similar to the one used to fabricate the HERA samples. The resulting rim thickness as a function of the hydrogen content is plotted in Fig. 3 and compared to the data provided by Nagase and Fuketa and to the expected rim thicknesses of the HERA cladding tubes.

### 2.2.2. Temperature dependency of the $f_2$ reduction factor

In the original formulation of the failure criterion, the ductility reduction factor due to hydrogen content $f_2$ is dependent on clad hydrogen content, temperature and strain rate (Table 2). The hyperbolic

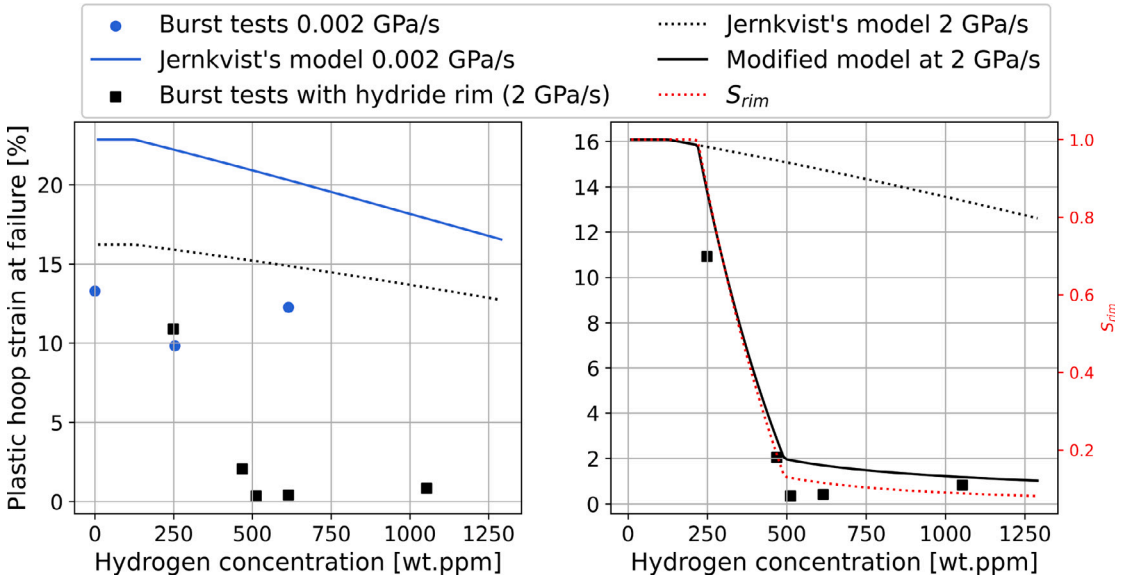


**Fig. 2.** Left: Plastic hoop strain at failure reported by Nagase and Fuketa (2005) for the burst tests conducted at 623 K. The lines plots correspond to the predicted failure strains according to the failure criterion proposed by Jernkvist et al. (2004). Right: Failure strains from the modified failure criterion for the burst tests that presented a hydride rim. The red dotted line shows a plot of the $S_{rim}$ reduction factor computed with Eqs. (8) to (10).

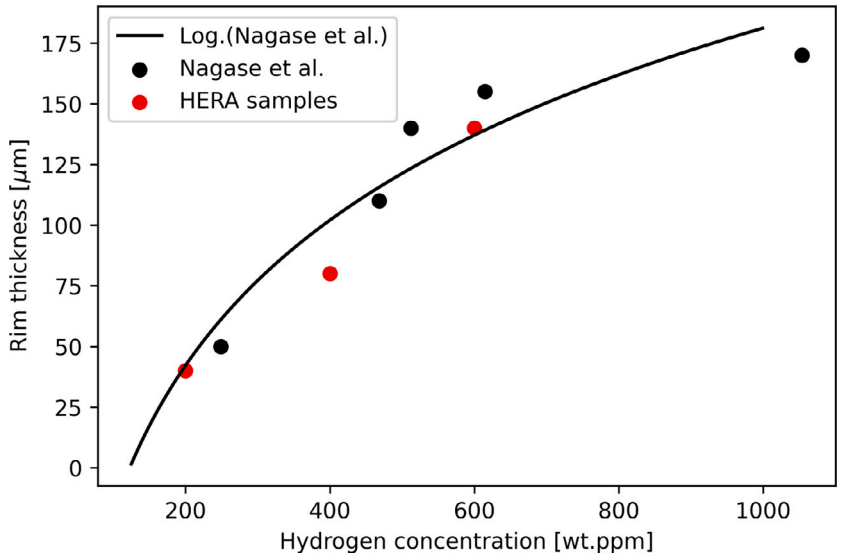


**Fig. 3.** Estimated hydride rim thickness as a function of the mean hydrogen content obtained with Eq. (11), compared with the rim thicknesses of the samples of Nagase and Fuketa (2005) and of the HERA test matrix (Table 3).

tangent of the $\gamma$ function considers a transition temperature of 298 K and a width factor ($wf$) of 8.5, leading to a quick recovery of the clad ductility above this temperature. Fig. 4 (left graph) shows the evolution of $f_2$ for a strain rate of 1 $s^{-1}$, an hydrogen concentration of 400 wt.ppm and a temperature ranging from 293 to 700 K, considering different values for the temperature of transition and width factor. As one can see, a transition temperature of 298 K with a width factor of 8.5 leads to a quasi complete recovery of the ductility at 325 K, whereas higher transition temperatures shift this recovery towards higher temperatures and higher width factor expand the temperature range on which recovery occurs. Based on the solubility limit of Kearns (1967) and assuming an instantaneous dissolution of hydrides, embrittlement due to the presence of solid hydrides cannot be recovered at temperatures below 450 K, temperature at which the solubility limit is close to 10 wt.ppm. Similarly, a width factor of 8.5 induces a rapid and illogical recovery in view of the terminal solubility limit. Thus, we consider hereafter a temperature of transition of 450 K and a width factor of 50 in the $\gamma$ function. This choice of parameters triggers recovery at 450 K that spans until 600 K, where the terminal solubility limit reaches 98 wt.ppm. The initial fit of Jernkvist et al. is probably due to the lack of out-of-pile experiments available between 300 and 550 K. To further support this modification of the $f_2$ function, the Critical Strain Energy Density (CSED) failure criterion proposed by Rashid and coworkers for low temperature RIA failure is considered valid up to 423 K (Rashid et al., 2001). Thus considering a temperature of transition at 450 K and a width factor of 50 is consistent with this criterion, as one can see on Fig. 4 (right graph), where low failure strains are obtained with both models at low temperatures (< 423 K), followed by a ductility recovery leading to high failure strains at high temperatures, above 550 K. It is interesting to note that our model predicts slightly higher failure strains at high temperatures. The methodology to convert the CSED criterion into an equivalent hoop plastic strain was proposed by Jernkvist and coworkers in their technical report (Jernkvist et al.,

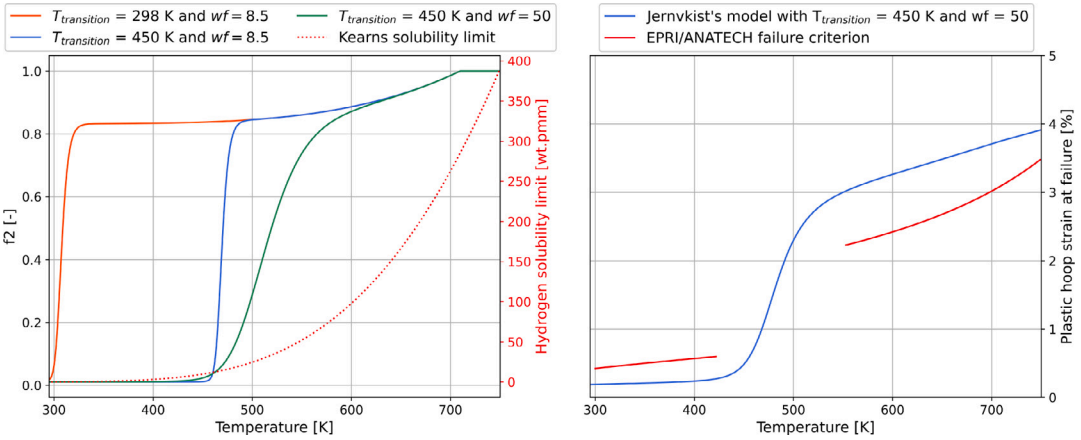


**Fig. 4.** Left graph: evolution of the $f_2$ ductility reduction factor as a function of temperature for different temperatures of transition in the $\gamma$ function. Strain rate is 1 $s^{-1}$ and average hydrogen content was set to 400 wt.ppm. Right graph: Evolution of the failure strain as a function of temperature according to the failure criterion considered in this study, based on Jernkvist et al. (2004), and of the CSED failure criterion of Rashid et al. (2001). Hoop strain rate was set to 0.5 /s, hydrogen content to 285 wt.ppm (corresponding to an oxide layer used in the EPRI model, of 40 μm). No effect of irradiation damage was considered.

2004) and is recalled in the Appendix section, as well as the correlations behind the CSED failure criterion (Rashid et al., 2001).

This modification of the $f_2$ reduction factor is important: during fast pulses starting from cold conditions such as the ones conducted at the NSRR facility, cladding can be mechanically loaded by PCMI and experience tensile loading before any real temperature increase.

## 3. Simulated HERA test cases

A total of four experiments are planned for the Phase 1 of the HERA project with two different pulse widths. From these four tests, two additional experimental parameters were selected to conduct a sensitivity study: the energy deposition and the hydrogen content/hydride rim thickness of the cladding tube. The final case matrix consists of 12 tests, with varying pulse width, energy deposition and hydrogen content/rim thickness (Jensen et al., 2023; Seo et al.).

The power pulses are assumed to follow a Gaussian time function as follows:

$$f(t) = \frac{1}{\sigma\sqrt{2\pi}} \exp\left(-\frac{1}{2}\frac{(t-t_m)^2}{\sigma^2}\right) \tag{12}$$

with $t_m$ the time of peak power that is set at 1.0 s. The pulse width was adjusted such that:

$$\sigma = \frac{\mathrm{FWHM}}{2\sqrt{2\ln(2)}} \tag{13}$$

and the magnitude of the pulse was scaled as needed to target the peak radial average enthalpy.

### 3.1. Description of the test rodlets

The test specimens are based on a standard 17 × 17 PWR fuel design, composed of a Zy-4 cladding and $UO_2$ fuel. One of the main objectives of this exercise being the investigation of the PCMI phase of the transient and failure of the cladding due to rapid loading and embrittlement by hydrogen pick-up and precipitation, the specimens were designed in order to reproduce important characteristics of irradiated fuel rods leading to strong PCMI and mechanical degradation of the cladding tubes. The former is obtained by using oversized fresh fuel pellets to reduce the fuel-gap size compared to the as-fabricated one. The latter is accomplished by hydrogenating the cladding tubes, thus inducing a solid hydride rim at the clad periphery with a thickness of around 80 μm and a nominal mean hydrogen concentration of 400 wt.ppm (Kamerman et al., 2023). The protocol is similar to the one used by Nagase and Fuketa for their test samples (Nagase and Fuketa, 2005). All the parameters of the 12 cases (pulse width, energy deposition, hydrogen content) are summarized in Table 3.

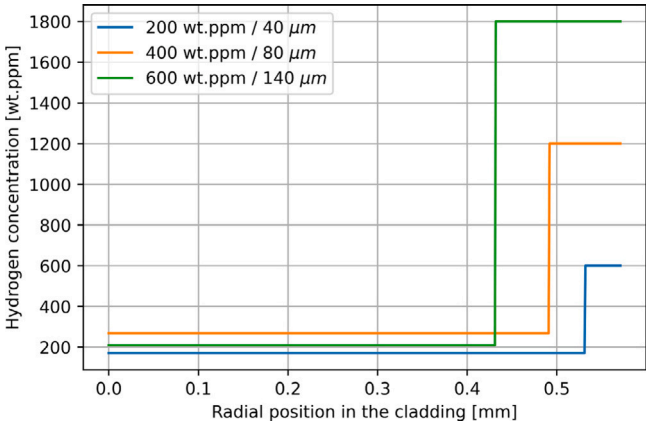


**Fig. 5.** Prescribed radial hydrogen concentration profiles in the simulations, depending on the average hydrogen content/rim thickness.

### 3.2. Hydrogen concentration profiles within the cladding

For these simulations, the radial concentration profiles of hydrogen in the cladding tubes were not available. Nagase and Fuketa (2005) indicated that hydrogen content in the hydride rim is roughly three times the mean hydrogen concentration of the cladding. We therefore assumed in the simulations that the rim hydrogen contents were equal to 3 times the hydrogen content given in Table 3. The hydrogen concentration beneath the rim is assumed constant and is set such that the mean hydrogen content of the cladding (200, 400 or 600 wt.ppm) is recovered in each case. The resulting radial profiles are plotted in Fig. 5.

## 4. OFFBEAT and ALCYONE fuel performance codes

### 4.1. OFFBEAT

Each case was simulated with OFFBEAT using a 2D-(rz) axisymmetric representation of the rodlet. The use of a 2D-(rz) scheme is

**Table 3**
Test matrix of the HERA M&S exercise considered in this study. The bold cases indicate the planned four experimental tests. The other cases were derived from these four tests for the M&S exercise.

| Case | Pulse width (FWHM) | Peak radial average enthalpy increase (J/g) | Hydrogen content /Rim thickness (ppm/μm) |
|---|---|---|---|
| **1** | | **650** | **400/80** |
| 2 | | 650 | 200/40 |
| 3 | 7.5 | 650 | 600/140 |
| 4 | | 550 | 400/80 |
| 5 | | 750 | 400/80 |
| **6** | | **650** | **400/80** |
| 7 | | 650 | 200/40 |
| 8 | 90 | 650 | 600/140 |
| 9 | | 550 | 400/80 |
| 10 | | 750 | 400/80 |
| **11** | 50 | **650** | **400/80** |
| **12** | 300 | **650** | **400/80** |

mandatory in OFFBEAT since the friction model at the pellet-clad interface is currently not available in 1.5D. The fuel was radially discretized in 44 cells progressively refined towards the outer periphery. A refined radial discretization of the cladding is needed to capture the radial concentration gradient of hydrogen. Thus, the cladding was discretized with 19 cells of equal volume, corresponding to a radial element size of about 27 μm. The fuel column was axially discretized into 12 axial slices (1 per pellet) and the cladding was axially discretized into 48 axial slices to maintain an aspect ratio below 5. The cladding in front of the cold plenum is also meshed with the same radial discretization and with an axial length consistent with the cold plenum volume. As OFFBEAT does not currently have a thermo-hydraulic solver, the external clad temperatures were calculated with ALCYONE and prescribed in the simulations. The following models or assumptions were also considered:

1. The fuel mechanical behavior is thermo-elastic.
2. The clad mechanical behavior is the viscoplastic model presented above.
3. The contact between the fuel and the cladding is handled with a penalty method. This method allows for the interpenetration of the fuel and clad meshes, leading to a contact pressure proportional to the penetration. A Coulomb friction model is used when the fuel-clad gap is closed. The friction coefficient was set equal to 1.
4. The rugosity at the fuel-clad interface is set at 0.1 μm on both sides. This assumption is consistent with the high contact pressures obtained during the PCMI phase of the transient (Moal et al., 2014). This value also ensures consistency with ALCYONE simulations used to prescribe cladding external temperatures.
5. A gap plenum model derived from FRAPCON is used to track the evolution of gap volume, pressure, temperature and conductance, taking into account gap-gas conductance, conductance due to radiative heat exchange and fuel-clad contact (Geelhood and Luscher, 2014).
6. Thermophysical properties for the cladding and the fuel are mainly from MATPRO (Hagrman and Reymann, 1979).

### 4.2. ALCYONE

Each case was simulated with ALCYONE with a 1.5D or 2D-(r$\theta$) representation of the rodlet. Guénot-Delahaie et al. (2018) presented the RIA related models of ALCYONE. In 1.5D, the fuel column was discretized with a single axial slice, as the power profile does not depend on the axial position and there is no coolant flow in the NSRR or TREAT test conditions. As for OFFBEAT, in ALCYONE 1.5D, the fuel was radially discretized in 44 elements with a progressive mesh refinement towards the outer periphery and the cladding was discretized with 19 elements of equal volume. The following models or assumptions were also considered:

1. The fuel mechanical behavior is viscoplastic with a Drucker–Prager yield criterion in compression and a smeared crack model to describe pellet cracking under tensile loading (Salvo et al., 2015b,a).
2. The clad mechanical behavior is the viscoplastic model presented above.
3. No axial sliding between the pellet and the cladding is allowed when the gap is closed.
4. The gap conductance model is based on the URGAP model (Lassmann and Hohlefeld, 1987).
5. ALCYONE solves the thermal and mass balance equations in the water coolant. The clad-to-water heat exchange coefficient is based on the clad-to-coolant heat flux correlations proposed by Bessiron (2007) and Bessiron et al. (2007). Regarding the clad-to-coolant heat exchange and the simulation of the boiling crisis for NSRR conditions, a readjustment of the parameters of the correlation has been recently proposed to improve calculations of film boiling durations (Guénot-Delahaie et al., 2022).

The 2D-(r$\theta$) scheme of ALCYONE (Sercombe et al., 2016) consists in a thermo-mechanical 2D generalized plane strain simulation of a pellet fragment representing one eighth of the pellet and of the overlying cladding (Fig. 6). At the pellet-clad interface, a Coulomb friction model is used with a friction coefficient of 0.5, valid for non-irradiated $UO_2$ (Sercombe et al., 2012). The treatment of the contact and friction in 2D-(r$\theta$) has been validated against closed-form solutions (Sercombe et al., 2013). The pellet-clad contact is treated implicitly in ALCYONE's thermo-mechanical solver (Cast3M, 2024) with the method of Lagrange multipliers that ensure the non-penetration of the pellet fragment and the re-opening of the pellet-clad gap. The cracking of a fictitious hydride blister or hydride rim of pre-determined thickness is considered in the 2D-(r$\theta$) by modifying the cladding mechanical boundary condition on the axis of symmetry of the pellet fragment (0x) during the simulation. Initially, the symmetry condition is enforced ($U_y = 0$). When a threshold hoop stress on the external cladding wall is reached, radial cracking of the blister is considered by applying an unilateral contact condition ($U_y \geq 0$) along the fictitious hydride blister, as represented in Fig. 6. The stress to failure of the hydride blister is 145 MPa, as deduced by Desquines et al. (2004) from experiments of the PROMETRA program (Cazalis et al., 2007). The deformation of the remaining clad ligament beneath the cracked rim due to the pellet thermal expansion and subsequent PCMI can thus be studied explicitly. Previous studies showed that plastic strains localize in a shear band oriented at 45° to the radial direction, starting from the crack tip (Sercombe et al., 2016). As the impact of rim thickness is explicitly considered in this scheme, the average plastic strain in the shear band after rim cracking is used to predict failure from the failure criterion proposed by Jernkvist et al. (2004), without the $S_{rim}$ reduction factor presented in Section 2.2.1. The results obtained with this scheme are used to validate those computed from 1.5D simulations with the $S_{rim}$ reduction factor.

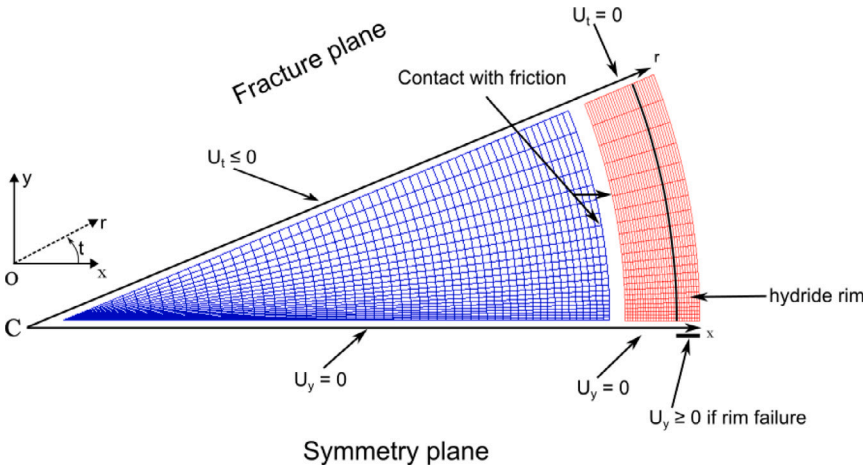


**Fig. 6.** Mesh and mechanical boundary conditions used in the 2D-(r$\theta$) scheme of ALCYONE.

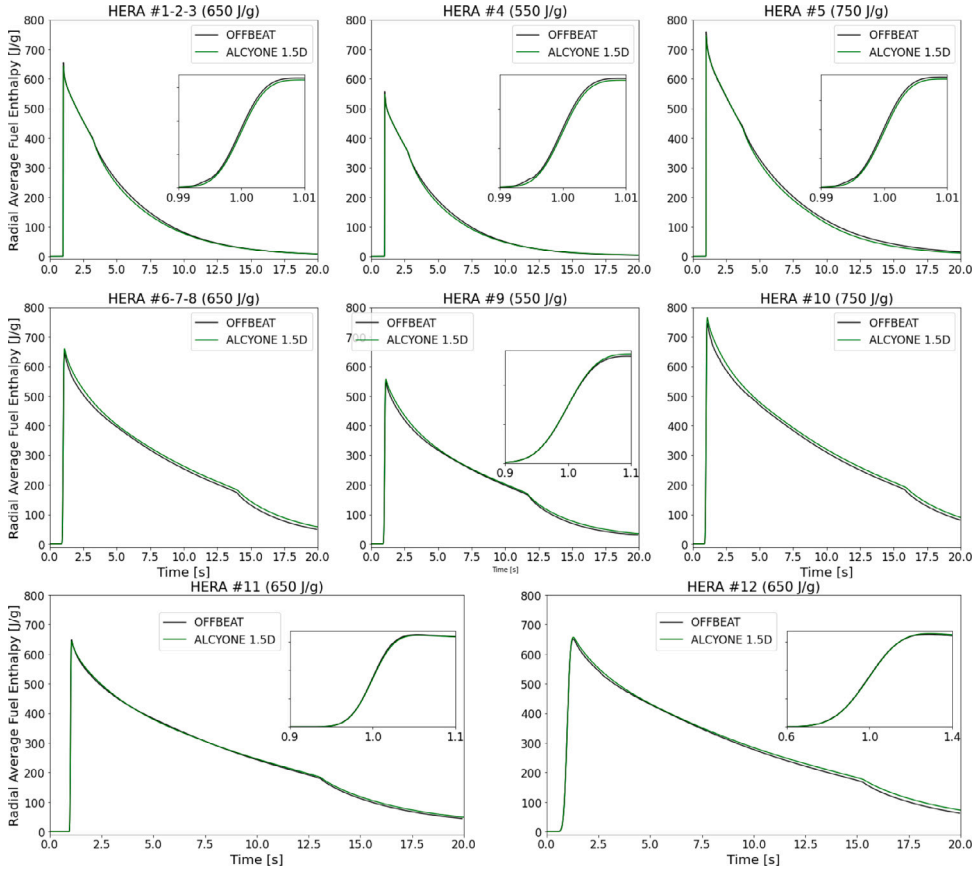


**Fig. 7.** Radial Average Fuel Enthalpies calculated with ALCYONE 1.5D and OFFBEAT. The insets show the discrepancies between the two codes during the heating phase of the transients.

## 5. Results

### 5.1. ALCYONE 1.5D and OFFBEAT thermal behavior

Regarding the thermal behavior of the fuel, the radial average peak enthalpies calculated by both OFFBEAT and ALCYONE (1.5D) are in agreement with the target values. The time evolutions of the radial average fuel enthalpy, calculated by the two codes for the 12 test cases, are plotted in Fig. 7. These results are in good agreement, with a maximum difference of around 10 J/g during the transients, confirming the quasi-identical thermal behavior of the fuel in the two codes. The small discrepancies can most likely be attributed to differences in the correlations used to model the heat capacity of the fuel in the two codes.

The time evolutions of the average cladding temperature are plotted in Fig. 8. The curves for the two codes are almost identical for all cases. In NSRR test conditions (7.5 ms FWHM, HERA-1 to 5), the calculated film boiling durations are between 2.5 and 4 s, depending on the injected energy. In TREAT test conditions (50, 90 or 300 ms FWHM, HERA-6 to 12), the calculated film boiling durations are between 11 and 15 s, also depending on the injected energy. The longer boiling duration obtained in TREAT conditions is due to the smaller diameter

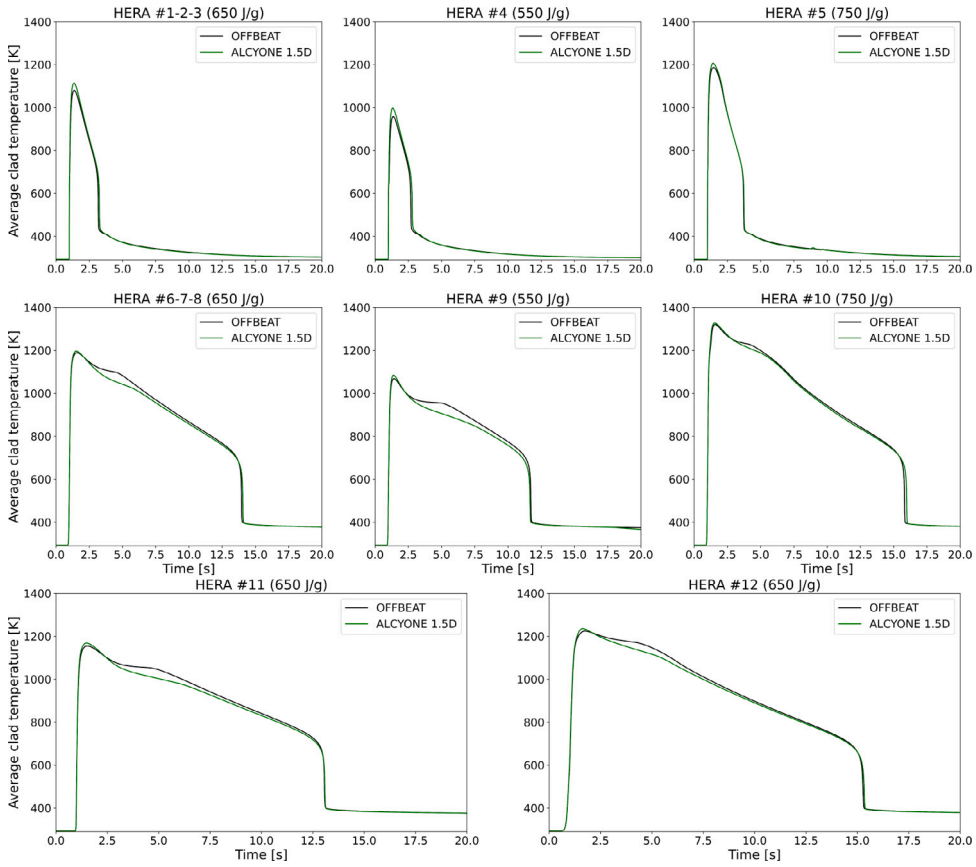


**Fig. 8.** Average clad temperatures calculated with ALCYONE 1.5D and OFFBEAT.

of the water capsule (25 mm) compared to NSRR (120 mm), leading to the boiling of the bulk of the water coolant.

### 5.2. Gap evolution and mechanical behavior of the cladding

Even though the cladding mechanical behavior is identical in ALCYONE and OFFBEAT, several differences appear in the simulations with the two codes related to the modeling hypotheses and the thermal mechanical models. Because OFFBEAT explicitly meshes the clad length in front of the plenum and prescribes the external cladding temperature calculated by ALCYONE, the plenum temperature is higher in OFFBEAT and the rod pressure is an order of magnitude higher in OFFBEAT ($\approx 1$ MPa) than in ALCYONE ($\approx 0.1$ MPa). The thermal strain models used for the fuel and the cladding in the two codes are slightly different. Finally, the fuel is thermo-elastic in OFFBEAT but viscoplastic in compression and elastic-brittle in tension in ALCYONE. As a result, the fuel deformation and the clad mechanical loading differ between the two codes.

The time evolutions of the gap width are plotted in Fig. 9. An earlier re-opening of the gap is obtained in OFFBEAT for the NSRR transients (HERA-1 to 5) and for HERA-11. The time evolutions of the calculated average total hoop strain in the cladding are plotted in Fig. 10. The expected trend of a higher hoop strain with increasing enthalpy deposition is obtained with both codes. For the NSRR pulses (HERA-1 to 5), OFFBEAT calculates a sharp increase of the total hoop strain after the first strain peak that corresponds to the earlier re-opening of the pellet-clad gap, whereas the strains calculated with ALCYONE decrease smoothly after the first strain peak . Despite these differences, the residual hoop strains are fairly close.

The time evolutions of the hoop stress at the cladding outer wall are plotted in Fig. 11. Overall, the peak hoop stresses of ALCYONE and OFFBEAT are consistent, indicating similar loading by the fuel pellets. For NSRR conditions (HERA-1 to 5), discrepancies between OFFBEAT and ALCYONE arise due to the earlier reopening of the fuel-clad gap in OFFBEAT, as indicated by the rapid drop after the peak stresses. For HERA-6 to HERA-11 pulses (90 or 50 ms FWHM), peak stresses are consistent, with a maximum difference of 115 MPa observed in the HERA-9 case. These discrepancies in terms of peak stresses can be explained by the use of a penalty method in OFFBEAT. The local contact pressure (Pa) applied when contact is detected between a fuel cell and a clad cell is given as:

$$p = -\left(\gamma \frac{A}{V} K\right) g \text{ [MPa]} \tag{14}$$

with A and V the fuel cell surface ($m^2$) and volume ($m^3$), K the fuel bulk modulus (MPa) and g the local gap width (m), negative in case of penetration. The resulting local interface pressure is proportional to the so-called *penalty scale factor* $\gamma$ that is an user defined parameter. The choice of the penalty factor is problem-dependent: a value too small can lead to significant interpenetration and to an unreliable solution while a high value can undermine numerical stability and introduce fluctuations or errors in the contact forces. In this study, the penalty factor was not adjusted on a case by case basis and was set to 0.1 as it ensured convergence without spurious oscillations for all cases while inducing a penetration that was reasonable (around 1 μm). As the penalty scalar factor value was found adequate for the short pulses leading to high contact pressures (up to 120 MPa for the HERA-5 case), it is not surprising that the calculation of the slowest pulse (HERA-12) seems to under-predict the applied contact pressure. Using a higher penalty scale factor for HERA-12 would certainly improve the comparison. The differences in the stresses can also explain part of the differences in total strains between the two codes. Furthermore,

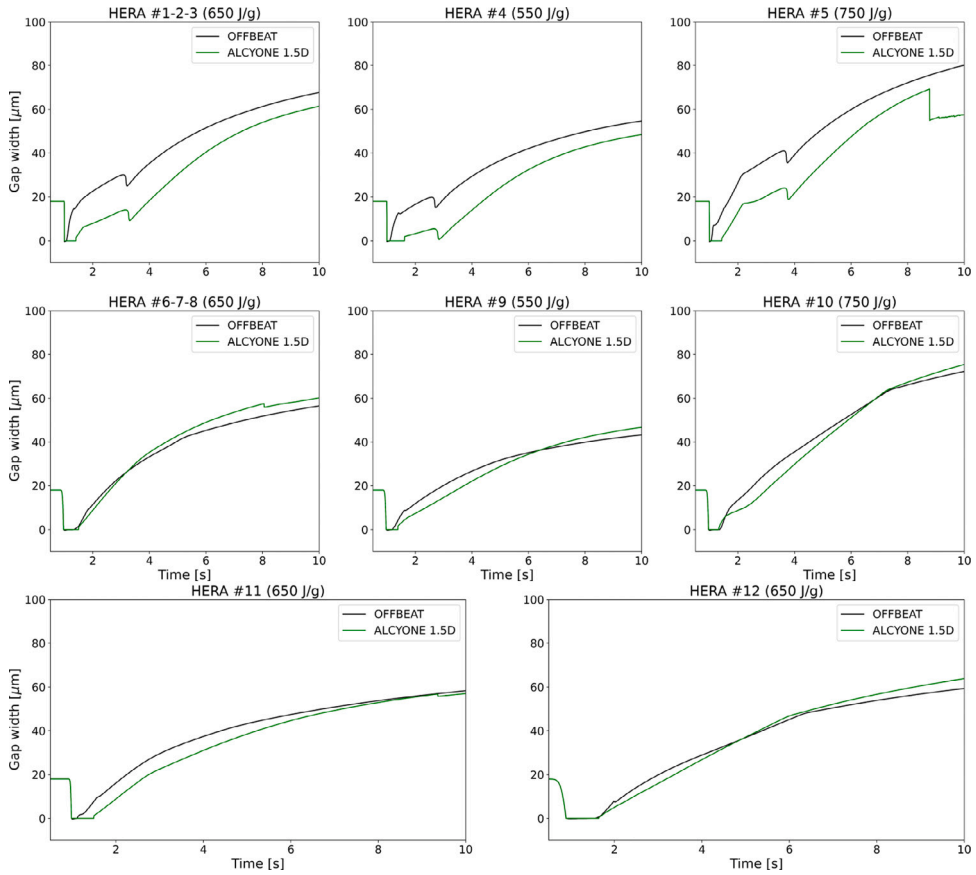


**Fig. 9.** Pellet-clad gap widths calculated with ALCYONE 1.5 and OFFBEAT.

the stress to failure of the hydride rim being ≈145 MPa (Desquines et al., 2004), the calculated hoop stresses show that the rim will fail during all the transients. The use of the 2D-(r, $\theta$) scheme where hydride rim failure is explicitly described is thus justified. Finally, the stress bi-axiality ratio $\left(\frac{\sigma_{zz}}{\sigma_{\theta\theta}}\right)$ during all transients is close to 1 with ALCYONE, due to the prescribed no sliding condition at the pellet-clad interface, and does not fall below 0.75 with OFFBEAT. These results align with those of Hellouin De Menibus et al. (2014) who estimated the stress bi-axiality ratio to be between 0.7 and 1 in the CABRI REP-Na transients, based on post-tests measurements. A stress bi-axiality ratio of 1 is assumed for the cladding failure assessment of the HERA tests that follows.

To conclude, while discrepancies exist between the two codes, the PCMI phase of the transients is nevertheless fairly similar in terms of strains and stresses reached in the cladding. An extensive parametric study considering each source of discrepancy one by one would be necessary to fully understand small differences between the code results.

### 5.3. ALCYONE 1.5D and OFFBEAT cladding failure assessment

Clad failure during the 12 test cases was estimated with the failure criterion proposed in Section 2.2.1. For both ALCYONE 1.5D and OFFBEAT, all the NSRR (HERA-1 to 5) pulses are predicted to fail. No failure is predicted for the TREAT pulses (HERA-6 to 12). The times, enthalpies and average cladding temperatures at failure are provided in Table 4. The time evolutions of the critical hoop plastic strain and of the average plastic strain in the cladding for HERA-1 to 3 and HERA-6 to 8 are plotted in Fig. 12. During the NSRR transients, the cladding underwent mechanical loading at low temperatures, where the hydrogen is still precipitated and the ductility of Zircaloy-4 is low. Failure thus occurred at low cladding average temperature (343–398 K, see Table 4). Conversely, during TREAT pulses (Fig. 12, bottom), cladding underwent mechanical loading at higher temperatures where ductility recovery had already begun, explaining why the critical hoop strain was not reached. Nevertheless, HERA-8 is close to failure with a ratio of hoop plastic strain and critical plastic strain close to 0.95 for both codes. A small variation (around 30 K) of the cladding temperature would have led to failure.

We compare the evolution of the time and enthalpy at failure during the NSRR pulses as a function of the rim thickness (40, 80, 140 μm) at constant peak enthalpy increase (650 J/g), corresponding to HERA-2, 1 and 3, and as a function of the peak enthalpy increase (550, 650, 750 J/g) at constant rim thickness (80 μm), corresponding to HERA-4, 1 and 5) in Figs. 13 and 14, respectively. The impact of the rim thickness is clearly visible in Fig. 13, with lower enthalpies and times at failure with increasing rim thickness. Regarding the impact of the injected energy, the time at failure decreases linearly with increasing power but the enthalpy at failure remains more or less the same. While the hoop strain rate increases with power, reaching a maximum of 2.15, 2.75 and 3.45 /s during HERA-4, 2 and 5, respectively, it has no effect on the enthalpy at failure because the $f_1$ reduction factor accounting for the effect of strain-rate on the ductility of Zy-4, is capped at 0.046 if the strain rate exceeds 1 /s (see Table 2).

Failures times are in excellent agreement between ALCYONE 1.5D and OFFBEAT with a maximum difference of 0.4 ms for HERA-2. The maximum difference on the enthalpy at failure is of 55 J/g for the same test, consistent with the difference in failure times. This maximum difference arises from the calculated hoop plastic strains between ALCYONE 1.5D and OFFBEAT, as one can see in Fig. 12. HERA-1 and 3 present less differences in the failure enthalpies since failure occurs earlier and the differences in plastic strains between the two codes are not as significant.

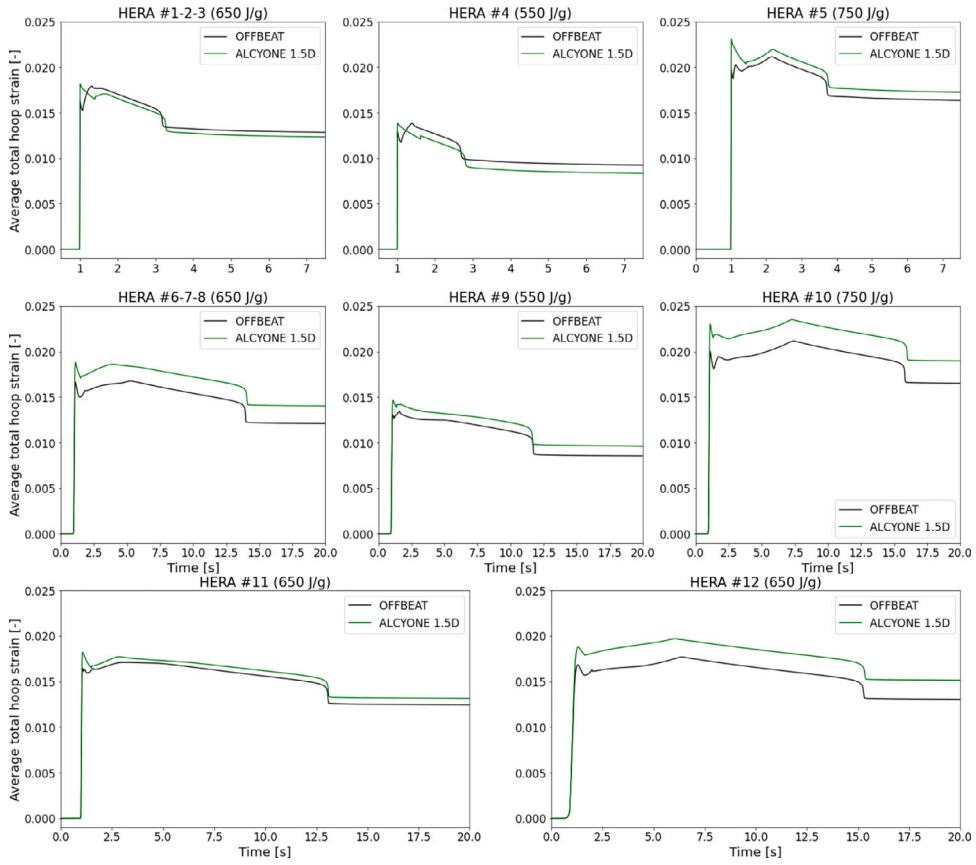


**Fig. 10.** Total hoop strains (thermal + mechanical) at the clad outer wall calculated with ALCYONE 1.5D and OFFBEAT.

**Table 4**
Times, average enthalpy increases and average clad temperatures at failure calculated with ALCYONE 1.5D and OFFBEAT.

| Case # | Failure time (s) | | Enthalpy at failure (J/g) | | Clad temperature at failure (K) | |
|---|---|---|---|---|---|---|
| | ALCYONE | OFFBEAT | ALCYONE | OFFBEAT | ALCYONE | OFFBEAT |
| 1 | 1.0002 | 1.0003 | 349 | 378 | 356 | 373 |
| 2 | 1.0008 | 1.0012 | 399 | 454 | 371 | 404 |
| 3 | 0.9995 | 0.9994 | 295 | 300 | 340 | 345 |
| 4 | 1.0010 | 1.0011 | 348 | 373 | 361 | 380 |
| 5 | 0.9996 | 0.9997 | 348 | 381 | 352 | 368 |

### 5.4. Comparison with ALCYONE 2D simulation results

Each case was also simulated with the 2D-(r$\theta$) scheme of ALCYONE. The cladding hoop plastic strains at failure times during the HERA-2, 1 and 3 tests are shown in Fig. 15. The impact of the hydride rim thickness is clearly seen with increasing strains reached at the tip of the cracked rim as its thickness increases. Also, a plastic strain localization in shear bands orientated at 45° with respect to the radial direction is visible in the uncracked ligament beneath the failed hydride rims. The failure criterion without the $S_{rim}$ reduction factor was used to assess failure during these simulations. To do so, the average quantities for the failure model (temperature, plastic strain and strain rate) were calculated along a line following the 45° shear band (black dotted lines, Fig. 15).

As in the simulations with ALCYONE 1.5D, all NSRR cases (HERA-1 to 5) led to clad failure while no failure was predicted for the TREAT cases. The impact of the hydride rim thickness can be seen in Fig. 16 where the time evolutions of the average hoop plastic strain calculated with ALCYONE in 1.5D and 2D-(r$\theta$) (in the shear band) are plotted for the 5 NSRR cases. It is clear that the plastic strain levels obtained with the 2D-(r$\theta$) scheme are consistently higher (more than twice) than those obtained with the 1.5D scheme. Moreover, thicker hydride rims lead to higher plastic strains in the shear band of the cladding with the 2D-(r$\theta$) scheme while this effect cannot be captured with the 1.5D scheme. As can be seen in Fig. 16 (left graph), the average plastic strains with ALCYONE 1.5D are the same for the HERA-1, 2, 3 cases (i.e., same peak enthalpy increase).

The times and enthalpies at failure calculated with ALCYONE 2D-(r$\theta$) are compared to ALCYONE 1.5D and OFFBEAT for the HERA-2, 1, 3 cases (increasing rim thickness) in Fig. 13 and in Fig. 14 for the HERA-4, 1, 5 cases (increasing peak enthalpy increase). The failure enthalpies obtained in all the simulations are given in Table 5 and, for the 1.5D simulations, are also expressed as a percentage of the enthalpies at failure obtained with the 2D-(r$\theta$) scheme of ALCYONE. The deviations on the calculated failure enthalpies between ALCYONE 1.5D and ALCYONE 2D-(r$\theta$) are below 10% for all cases. The deviations between OFFBEAT and ALCYONE 2D-(r$\theta$) are below 25% for all cases. The differences between ALCYONE 1.5D and 2D-(r$\theta$) results are acceptable with small variations on the expected failure times, ranging from 0.2 to 0.4 ms.

### 5.5. Comparison with previous NSRR experiments

As all NSRR transients are expected to result in failure, it is interesting to compare our results with the previously published results of

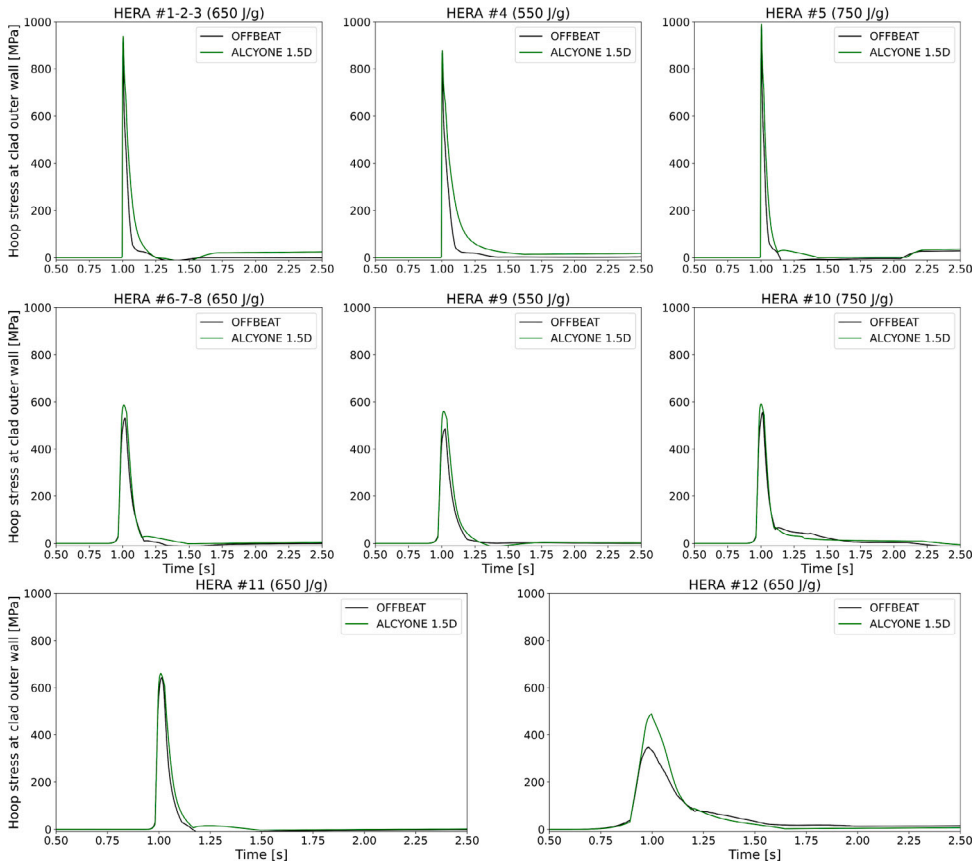


**Fig. 11.** Hoop stresses at the clad outer wall calculated with ALCYONE 1.5D and OFFBEAT.

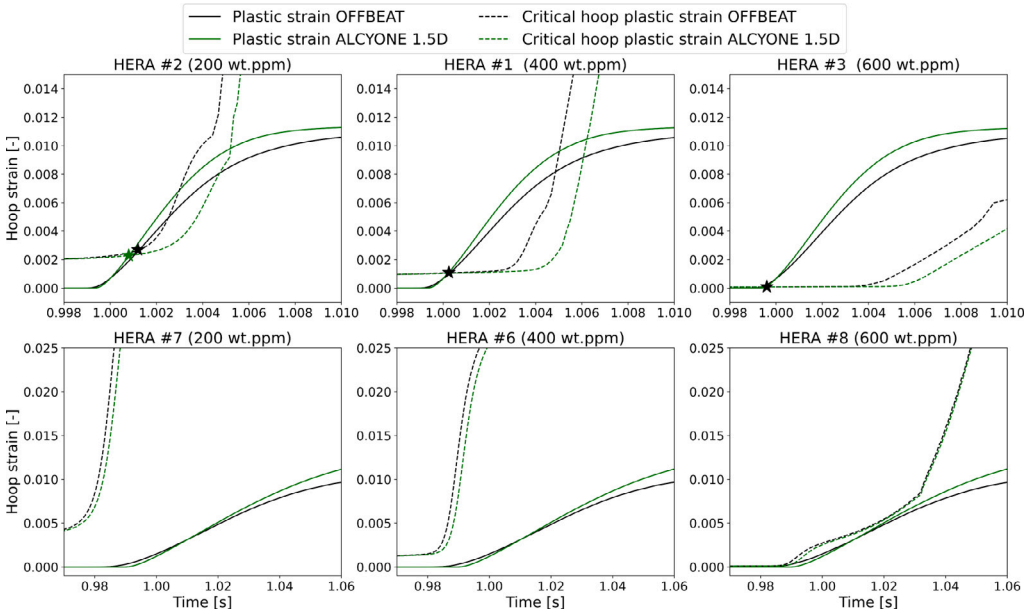


**Fig. 12.** Average plastic strains (solid lines) and critical hoop strains (dashed lines) calculated with OFFBEAT and ALCYONE 1.5D for the NSRR (top) and TREAT (bottom). Test cases with a 650 J/g enthalpy increase. Cladding failures during NSRR transients are indicated with a star.

NSRR transients conducted on unirradiated fuel rods with artificially hydrided cladding, as detailed by Tomiyasu et al. (2007). The enthalpies at failure as a function of the hydride rim thickness reported by Tomiyasu et al. are compared to our results in Fig. 17. As the enthalpies at failure are not very dependent on the peak enthalpy increase, we only plotted the results from the 650 J/g test cases (HERA-1, 2, 3). The gray area corresponds to the dispersion of the results reported by Tomiyasu et al. assuming that the enthalpy at failure is proportional to the inverse of the square root of the hydride rim thickness. One should note the strong dispersion of results in the experiments of Tomiyasu et al. that can be attributed to the uncertainty on the determination of the hydride rim thickness. As one can see, our results are consistent

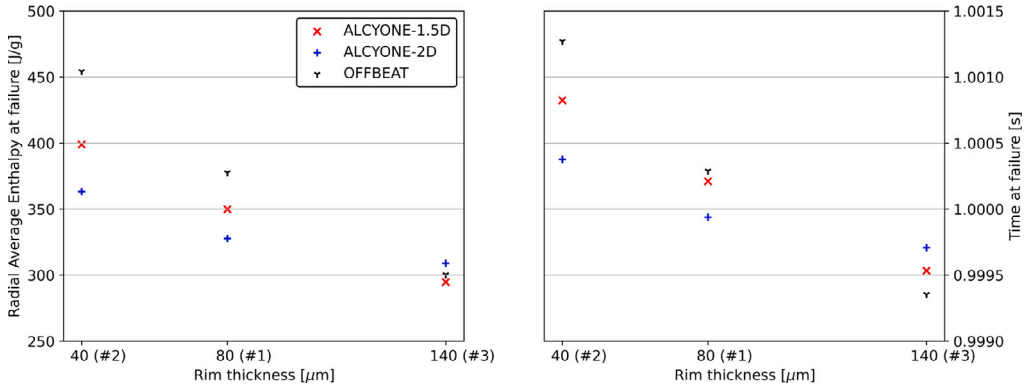


**Fig. 13.** Impact of the rim thickness on cladding failure in NSRR tests. Left: calculated enthalpies at failures obtained with ALCYONE and OFFBEAT. Right: corresponding failure times.

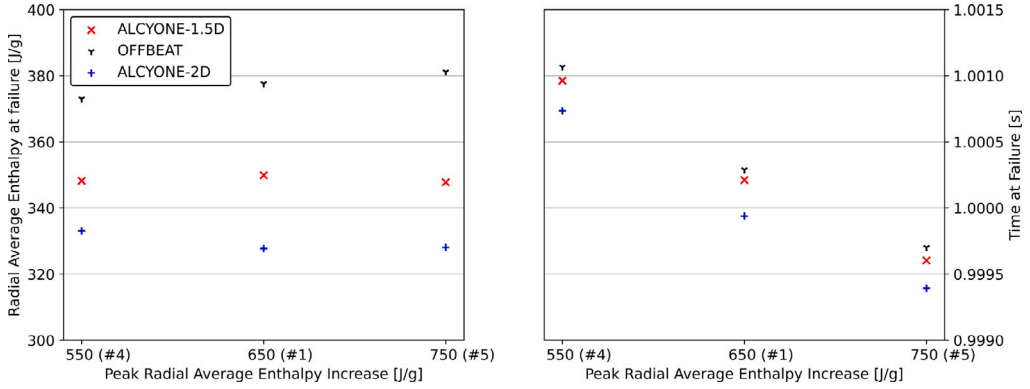


**Fig. 14.** Impact of the peak radial average enthalpy increase. Left graph: calculated enthalpies at failure obtained with ALCYONE and OFFBEAT. Right graph: corresponding failure times.

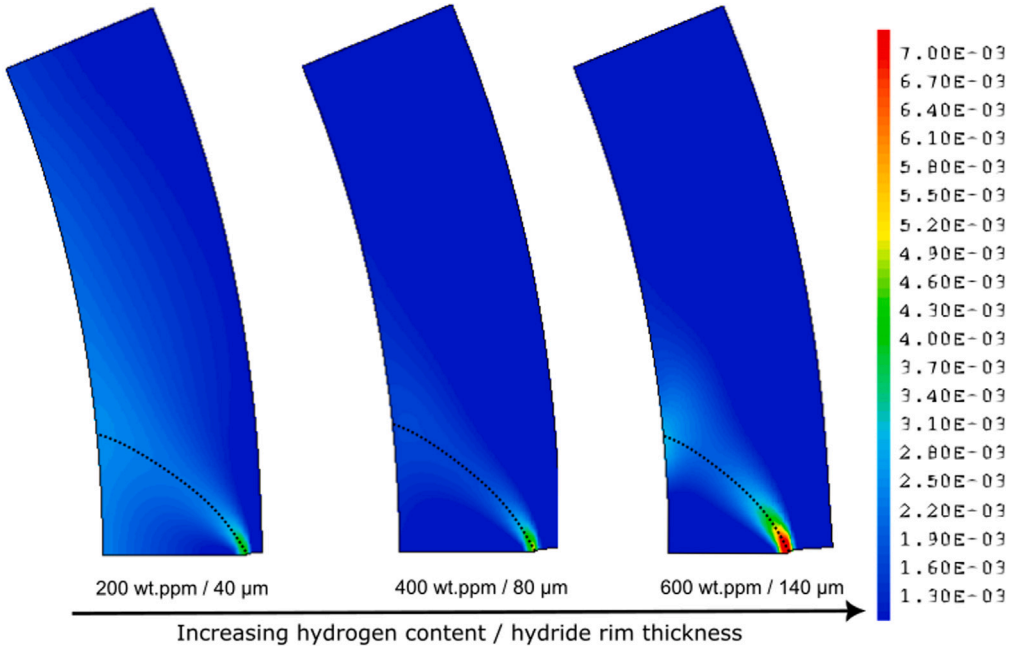


**Fig. 15.** Circumferential hoop plastic strains obtained with the 2D-r$\theta$ scheme of ALCYONE at the time of failure during the HERA-2,1,3 cases (left to right). The black dotted lines indicate where the average quantities for the failure criterion are calculated.

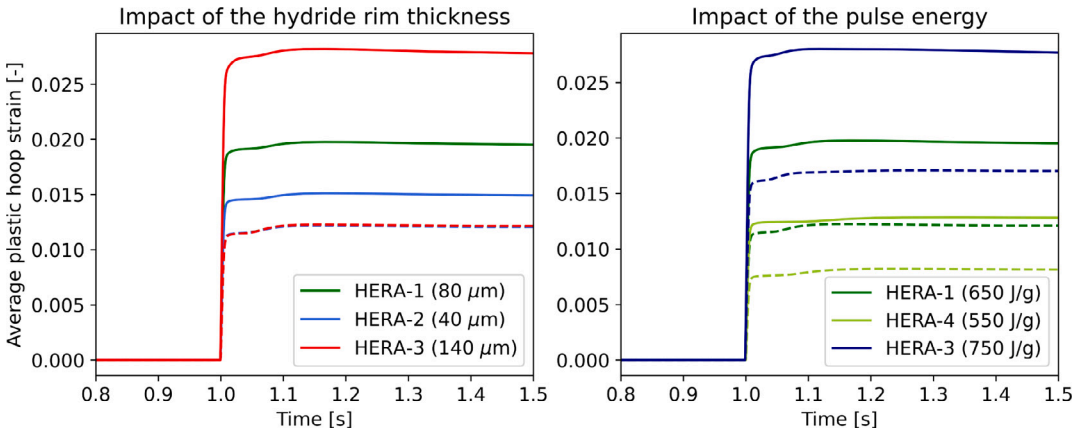


**Fig. 16.** Average hoop plastic strains in the cladding calculated for the NSRR pulses with ALCYONE 2D-(r$\theta$) (solid lines) and 1.5D (dashed lines).

**Table 5**
Calculated failure enthalpies (J/g). For ALCYONE 1.5D and OFFBEAT simulations, the % columns indicate the failure enthalpies as a % of those calculated in 2D-($r\theta$).

| Case # | ALCYONE 2D-($r\theta$) | ALCYONE 1.5D | % | OFFBEAT | % |
|---|---|---|---|---|---|
| 1 | 328 | 350 | 107 | 378 | 115 |
| 2 | 363 | 399 | 110 | 454 | 125 |
| 3 | 309 | 295 | 95 | 300 | 97 |
| 4 | 333 | 348 | 105 | 373 | 112 |
| 5 | 328 | 348 | 106 | 381 | 116 |

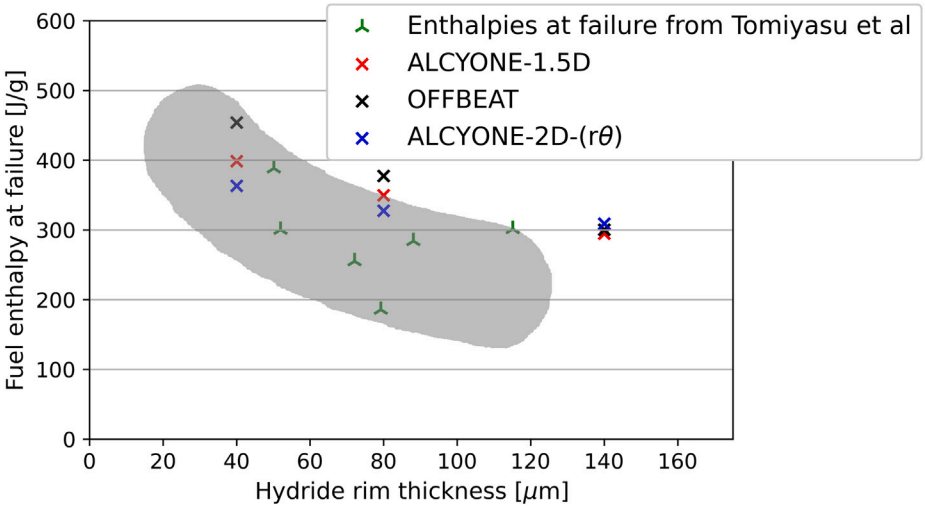


**Fig. 17.** NSRR enthalpies at failures reported by Tomiyasu et al. (2007) and obtained in this study as a function of the hydride rim thickness.

with those of Tomiyasu et al. and the decrease of the enthalpy at failure with increasing rim thickness is qualitatively well reproduced with the three simulation schemes presented in this study.

### *5.6. Discussion on the validity of the proposed failure criterion at high temperatures*

The failure criterion proposed in Section 2.2 is based on the introduction of a clad ductility reduction factor dependent on the rim thickness. This factor was calibrated using burst tests conducted by Nagase and Fuketa (2005) at room temperature and at 623 K on pre-hydrided samples. Comparisons between OFFBEAT and ALCYONE 1.5D simulations considering this reduction factor and the 2D-(r, $\theta$) scheme of ALCYONE simulating explicitly the hydride rim failure during the fast HERA cases yielded consistent results, thus indicating that the low temperature ($<$ 373 K) PCMI failure is well assessed. This approach leads to consistent estimations of the failure enthalpies compared to those previously reported by Tomiyasu et al. (2007).

Failure is not reached during slower transients (HERA-6 to 12), as cladding undergoes PCMI and plastic deformation at higher temperatures. As illustrated in Fig. 18, failure is however almost reached in HERA-8 with ALCYONE 1.5D or OFFBEAT while it is clearly not the case with ALCYONE 2D-(r$\theta$). This is due to the ductility recovery kinetics that depends on the fraction of dissolved hydrogen at the crack tip in the $S_{rim}$ reduction factor while the model used in ALCYONE 2D-(r$\theta$) only considers the recovery induced by the $f_2$ reduction factor (see Table 2 and Fig. 4). Using the temperature at the crack tip in the $S_{recovery}$ is representative of the expected behavior of hydrided Zy-4 cladding, as the $S_{rim}$ factor is meant to represent the loss of ductility induced by a cracked rim. On this topic, Udagawa et al. (2014) used a damage model to simulate the fracture behavior of Zy-4 cladding under RIA conditions. According to their findings, the failure strain was around 30% higher when the temperature radial gradient in the

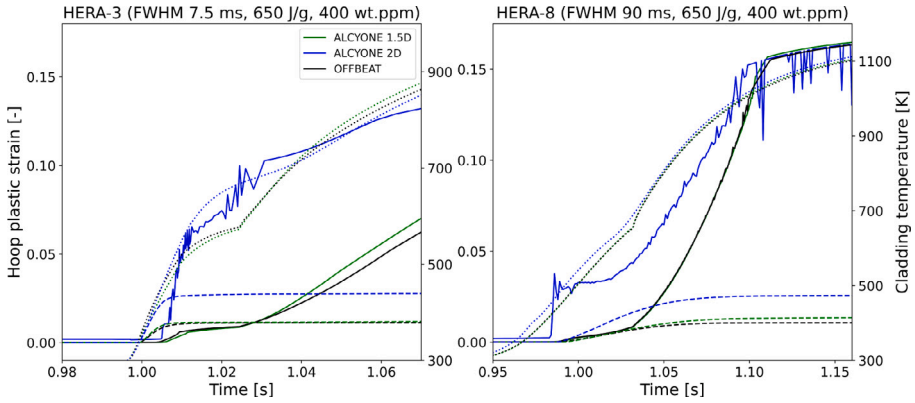


**Fig. 18.** Calculated time evolutions of the plastic strain (solid lines, left axis), of the critical hoop plastic strain (dashed lines, left axis) and of the cladding temperature (dotted lines, right axis) by each code during the HERA-3 and HERA-8 test cases. For OFFBEAT and ALCYONE 1.5D, the cladding temperature is the crack tip temperature. For ALCYONE 2D-(r$\theta$), the cladding temperature is the average temperature in the shear band.

cladding was taken into account than when the temperature profile was flat. Similarly, Tomiyasu et al. (2007) concluded that the stress intensity factor at failure (given as $K_{IC} = \frac{\sigma_{\theta\theta}}{\sqrt{\pi a}}$, with $\sigma_{\theta\theta}$ the hoop tensile stress at failure in MPa and $a$ the depth of the crack in m, corresponding to the thickness of the hydride rim) is higher when the average cladding temperature at failure is higher. Thus, it is expected that cladding can support larger PCMI loading in transient conditions allowing time for temperature increase prior to experiencing a tensile load, as in TREAT conditions. Furthermore, studies of the stress intensity factor of delayed hydride cracking (DHC) in Zircaloy-4 cladding reported that the stress intensity factor at which the initial crack grows for hydrided Zy-4 samples increases with temperature, especially above 600 K (Alvarez Holston and Stjärnsäter, 2017; Colldeweih and Bertsch, 2022; Hong et al., 2021). Our approach reproduces this behavior fairly well. As seen in Fig. 18, the critical hoop strain increases when the crack tip temperature exceeds 600 K. The ductility recovery process could also take place below 600 K, as suggested by recent burst test results conducted on hydrided cladding tubes similar to the ones used in the HERA project. Kamerman et al. (2023) reported failure strain of around 0.3 % at room temperature to around 2.5% at 150 K for hydrogen concentrations between 250 and 400 ppm. These tests were however conducted at low strain rates. More data and testing is necessary to determine the evolution of hydrided Zy-4 failure as a function of temperature.

The rim thickness is also inherently difficult to define and accurately measure, and it can also vary axially or azimuthally for a given specimen. Kamerman et al. (2023) reported a significant dispersion of the hydride rim thickness for samples hydrided with the same protocol as the one used for producing the HERA samples, with hydride thicknesses ranging from 60 to 100 μm. In this regard, the HERA-1 to 3 and HERA-6 to 8 are thought to be representative of the expected dispersion of the hydride rim thickness in the cladding of the HERA tests. For instance, the hydride rim thickness as a function of the mean hydrogen concentration of the cladding given by Tomiyasu et al. (2007) present an important dispersion in regard to the trend depicted in Fig. 3.

Concerning the minimal value of the $S_0$ factor, currently set at 0.05 (see Eq. (9)), Hellouin de Menibus et al. (2014) conducted bi-axial mechanical tests on Zircaloy-4 samples with a pre-formed hydride blister and reported the evolution of the failure strain as a function of temperature and blister depth. For a blister depth of 120 μm and a temperature of 623 K, the reported failure strain was around 10%. This is far more than the 1% failure strain measured during burst tests on pre-hydrided samples by Nagase and Fuketa (2005). This indicates that the choice of the $S_0$ factor should be based on experimental data as representative as possible of the bi-axial loading conditions during a RIA.

## 6. Conclusions

In this paper, cladding failure by PCMI during a RIA was studied with two fuel performance codes, OFFBEAT and ALCYONE, in the framework of the HERA project (NEA HERA, 2024). As the specimens are made of unirradiated fuel rods with artificially hydrided cladding tubes, an anisotropic mechanical model suitable for these non homogeneous materials (Le Saux et al., 2015) was implemented into both codes to simulate with accuracy the clad mechanical behavior. In order to assess clad failure with ALCYONE 1.5D and OFFBEAT, we proposed an extension of the failure criterion of Jernkvist et al. (2004), to take into account the thickness of the hydride rim that plays a critical role in the failure of the cladding during the transient. Both codes yielded similar results regarding the assessment of cladding failure with small discrepancies on the enthalpies at failure. We believe these differences arise mainly from the different contact algorithms used in OFFBEAT and ALCYONE and from the different thermo-mechanical models used for the fuel.

The extension of Jernkvist's failure criterion to include a hydride rim dependency and the results it yielded were compared with those obtained with ALCYONE 2D-(r$\theta$). This scheme explicitly takes into consideration the rim thickness by locally modifying the boundary conditions in the rim when a failure stress threshold -corresponding to the failure stress of a hydride rim- is reached. The two dimensional simulations yielded plastic strains greater than in 1.5D. During fast pulses (FWHM 7.5 ms, NSRR conditions), the times and enthalpies at failure obtained with ALCYONE 1.5D and 2D-(r$\theta$) are consistent, which validates the proposed modified failure criterion for NSRR conditions. For larger pulses widths (50–300 ms, TREAT conditions), results are also consistent, with no clad failures predicted as cladding undergoes mechanical tensile loads at high temperatures ($>$ 500 K) at which cladding ductility recovery occurs.

The analysis of the experimental results of the HERA tests with this criterion will be of great interest to better assess the PCMI failure during fast and slow transients. Furthermore, the planned measurements of the hydrogen radial profile in the cladding will provide valuable information regarding the state of the cladding before and after the tests (potential hydride dissolution) performed in the TREAT facility.

Access to the radial hydrogen profile could also improve the simulations by allowing a more precise description of the clad mechanical behavior. On this topic, recent works have been published on hydrogen transport and hydride precipitation within the cladding and the proposed models and methodologies could be coupled with our approach to simulate accurately the hydride distribution within the clad before the transient simulations (Nantes et al., 2024). To conclude, one of the recommendation of the synthesis report of the phase III of the NEA

RIA benchmark was the improvement of cladding failure criteria (NEA - Working Group on Fuel Satefy, 2022b). This study constitutes an attempt in doing so.

Finally, this study is also the first use of OFFBEAT for the simulations of RIA and the implementation of its new capacities have been verified by comparison with a well established fuel performance code validated on numerous experimental results. As OFFBEAT is a free open-source code, these developments and capabilities are now available to the fuel performance community. Regarding the contact algorithm, ongoing work aims at improving the implicit contact algorithm for open/close gap scenarii like those encountered in this study (Scolaro et al., 2022b). Additionally, ongoing and future work aim at implementing capabilities regarding irradiated fuel rods, such as transient Fission Gas Release (Reymond et al., 2024) or the coupling with the Gen-FOAM thermo-hydraulic solver (Fiorina et al., 2015) which is also based on the OpenFOAM library.

The modeling of crack initiation and propagation within the cladding wall is also planned in ALCYONE by using a Gurson–Tvergaard–Needleman damage model (Le Saux et al., 2015). These developments aim at removing the need for a failure criterion dependent on the rim or blister thickness which is intrinsically difficult to define and accurately measure.

## CRediT authorship contribution statement

**Matthieu Reymond:** Writing – review & editing, Writing – original draft, Software, Methodology, Investigation, Conceptualization. **Jérôme Sercombe:** Writing – review & editing, Validation, Software, Investigation, Conceptualization. **Alessandro Scolaro:** Writing – review & editing, Validation, Software, Conceptualization.

## Declaration of competing interest

The authors declare that they have no known competing financial interests or personal relationships that could have appeared to influence the work reported in this paper.

## Data availability

The data that support the findings of this study are available from the corresponding author upon reasonable request.

OFFBEAT is a free open-source fuel performance code available at: https://gitlab.com/foam-for-nuclear/offbeat.

## Acknowledgments

The authors would like to thank Colby B. Jensen, Charles P. Folsom and Seokbin Seo from the Idaho National Laboratory for the organization of this Modeling and Simulation exercise.

This work has received funding from the Jules Horowitz Reactor and CRAYON projects of CEA. Support from Gilles Bignan and Chrystelle Nonon-Solaro is gratefully acknowledged. This work has received funding from the Swiss Federal Office of Energy. This work has received funding from the Euratom research and training programme 2021–2027 through the OperaHPC project under grant agreement n° 101061453. Views and opinions expressed in this paper reflect only the authors' view and neither the European Commission nor the Swiss Federal Office of Energy are responsible for any use that may be made of the information it contains.

Reviewers are gratefully acknowledged for providing valuable insights and comments that have greatly improved the content of the paper.

## Appendix. Critical strain energy density correlation by EPRI/ANATECH

The correlation for critical strain energy density (CSED) proposed by Rashid et al. (2001) is given by:

$$CSED = C_1 e^{-C_2 x} \tag{15}$$

where $x$ is clad outer oxide layer thickness to the clad wall thickness ratio. $C_1$ and $C_2$ are given for two non-continuous temperature intervals, based on the experimental database used to determine these correlations:

For $295 < T < 423$ K:

$$C_1 = 15.6, \quad C_2 = 7.17 \tag{16}$$

For $553 < T < 673$ K:

$$C_1 = 41.5, \quad C_2 = 6.62 \tag{17}$$

*CSED to hoop failure strain*

The relation between critical strain energy density and hoop failure was detailed by Jernkvist et al. in their report (Jernkvist et al., 2004). It can be expressed as follows:

$$\varepsilon_f = \frac{1}{2}\left[\left(\frac{\sigma_y}{E}\right)^{n+1} + \frac{(n+1)\left(CSED - \frac{\sigma_y^2}{2E}\right)}{\sigma_y^{(1-n)} E^n}\right]^{\frac{1}{1+n}} - \frac{\sigma_y}{2E} \tag{18}$$

With the yield stress $\sigma_y$ given by:

$$\sigma_y = \left[\frac{K}{E^n}\left(\frac{2\dot{\varepsilon}_{\theta\theta}}{\dot{\varepsilon}_0}\right)^m\right]^{\frac{1}{1-n}} \tag{19}$$

It is based on the MATPRO correlations for material properties (Hagrman and Reymann, 1979). Strain rate dependence of the yield stress is defined by two constants:

$$\dot{\varepsilon}_0 = 1.10^{-3} \quad \left[\mathrm{s}^{-1}\right] \tag{20}$$

$$m = 0.02 \tag{21}$$

The strain hardening coefficient $n$ is a function of temperature:

$$n = -9.49 \cdot 10^{-2} + T\left[1.165 \cdot 10^{-3} + T\left(9.588 \cdot 10^{-10} - 1.992 \cdot 10^{-6}\right)\right) \tag{22}$$

The strength coefficient is dependent on temperature and fast (≥1 MeV) neutron fluence $\phi$ ($\mathrm{m}^{-2}$), so that:

$$K = K_T + K_\phi \quad [\mathrm{Pa}] \tag{23}$$

with the temperature dependant part given by:

$$K_T = 1.17628 \cdot 10^9 + T\left[4.54859 \cdot 10^5 + T\left(1.72752T - 3.28185 \cdot 10^3\right)\right] \quad [\mathrm{Pa}] \tag{24}$$

and the irradiation dependant part given by:

$$K_\phi = 5.54 \cdot 10^{-18}\phi \quad [\mathrm{Pa}] \tag{25}$$

Finally, the elastic modulus is given by:

$$E = \frac{1.088 \cdot 10^{11} - 5.475 \cdot 10^7 T}{0.88 + 0.12e^{-1 \cdot 10^{-25}\phi}} \quad [\mathrm{Pa}] \tag{26}$$

## References

Alvarez Holston, A.M., Stjärnsäter, J., 2017. On the effect of temperature on the threshold stress intensity factor of delayed hydride cracking in light water reactor fuel cladding. Nucl. Eng. Technol. 49, 663–667. http://dx.doi.org/10.1016/j.net.2017.04.002.

Andersson, T., Wilson, A., 1979. Ductility of zircaloy canning tubes in relation to stress ratio in biaxial testing. ASTM Special Tech. Publ. 60–71. http://dx.doi.org/10.1520/STP36672S, https://www.astm.org/stp36672s.html.

Bessiron, V., 2007. Modelling of clad-to-coolant heat transfer for RIA applications. J. Nucl. Sci. Technol. 44, 211–221. http://dx.doi.org/10.1080/18811248.2007.9711275.

Bessiron, V., Sugiyama, T., Fuketa, T., 2007. Clad-to-coolant heat transfer in NSRR experiments. J. Nucl. Sci. Technol. 44, 723–732. http://dx.doi.org/10.1080/18811248.2007.9711861.

Brunetto, E.L., Scolaro, A., Fiorina, C., Pautz, A., 2023. Extension of the OFFBEAT fuel performance code to finite strains and validation against LOCA experiments. Nucl. Eng. Des. 406, 112232. http://dx.doi.org/10.1016/J.NUCENGDES.2023.112232.

Cast3M, 2024. Cast3M. https://www-cast3m.cea.fr/.

Cazalis, B., Desquines, J., Poussard, C., Petit, M., Monerie, Y., Bernaudat, C., Yvon, P., Averty, X., 2007. The PROMETRA program: Fuel cladding mechanical behavior under high strain rate. Nucl. Technol. 157, 215–229. http://dx.doi.org/10.13182/NT07-A3814.

Chung, H.M., Kassner, T.F., 1998. Cladding metallurgy and fracture behavior during reactivity-initiated accidents at high burnup. Nucl. Eng. Des. 186, 411–427.

Colldeweih, A.W., Bertsch, J., 2022. Effect of temperature and hydrogen concentration on the threshold stress intensity factor of radial delayed hydride cracking in fuel cladding. J. Nucl. Mater. 565, 153737. http://dx.doi.org/10.1016/j.jnucmat.2022.153737.

Courty, O., Motta, A.T., Hales, J.D., 2014. Modeling and simulation of hydrogen behavior in zircaloy-4 fuel cladding. J. Nucl. Mater. 452, 311–320. http://dx.doi.org/10.1016/j.jnucmat.2014.05.013.

D'Ambrosi, V., Sercombe, J., Béjaoui, S., Zacharie-Aubrun, I., Introïni, C., Karlsson, J., Jädernäs, D., Zwicky, H.U., 2023. Presentation of the xM3 test case of the P2M simulation exercise and modeling with the fuel performance code ALCYONE. Nucl. Technol. 210, 285–307. http://dx.doi.org/10.1080/00295450.2023.2253660.

Desquines, J., Cazalis, B., Bernaudat, C., Poussard, C., Averty, X., Yvon, P., 2004. Mechanical properties of zircaloy-4 PWR fuel cladding with burnup 54-64MWd/kgU and implications for RIA behavior. In: Proceedings of the ASTM conference on Zirconium in the Nuclear Industry, Stockholm, Sweden.

Fiorina, C., Clifford, I., Aufiero, M., Mikityuk, K., 2015. GeN-foam: A novel OpenFOAM® based multi-physics solver for 2D/3D transient analysis of nuclear reactors. Nucl. Eng. Des. 294, 24–37. http://dx.doi.org/10.1016/J.NUCENGDES.2015.05.035.

Folsom, C., Seo, S., Kamerman, D., Jensen, C., 2023. HERA modeling and simulation exercise : BISON results. In: ANS Winter Conference and Expo November 12–15, Washington, D.C.. pp. 532–535.

Fuketa, T., Sasajima, H., Mori, Y., Ishijima, K., 1997. Fuel failure and fission gas release in high burnup PWR fuels under RIA conditions. J. Nucl. Mater. 248, 249–256.

Fuketa, T., Sugiyama, T., Nagase, F., 2006. Behavior of 60 to 78MWd/kgU PWR fuels under reactivity-initiated accident conditions. J. Nucl. Sci. Technol. 43, 1080–1088. http://dx.doi.org/10.1080/18811248.2006.9711198.

Geelhood, K.J., Luscher, W.G., 2014. NUREG/CR-7022 Vol 1 Rev 1 FRAPCON-3.5: A Computer Code for the Calculation of Steady-State, Thermal-Mechanical Behavior of Oxide Fuel Rods for High Burnup. Technical Report, PNNL.

Germain, A., Sercombe, J., Riglet-Martial, C., Introïni, L., Pontillon, Y., Maugis, P., 2022. Modeling of fission product release during severe accidents with the fuel performance code ALCYONE. Nucl. Eng. Des. 393, http://dx.doi.org/10.1016/J.NUCENGDES.2022.111778.

Guénot-Delahaie, I., Sercombe, J., Federici, E., Bernaudat, C., Largenton, R., Haller, X., 2022. Investigation of clad ballooning during NSRR RIA tests using ALCYONE fuel performance code. J. Nucl. Mater. 562, 153584. http://dx.doi.org/10.1016/j.jnucmat.2022.153584.

Guénot-Delahaie, I., Sercombe, J., Helfer, T., Goldbronn, P., Federici, E., Le Jolu, T., Parrot, A., Delafoy, C., Bernaudat, C., 2018. Simulation of reactivity-initiated accident transients on UO2-M5®fuel rods with ALCYONE V1.4 fuel performance code. Nucl. Eng. Technol. 50, 268–279. http://dx.doi.org/10.1016/j.net.2017.12.006.

Hagrman, D., Reymann, G., 1979. MATPRO-Version 11: A Handbook of Materials Properties for Use in the Analysis of Light Water Reactor Fuel Rod Behavior. Technical Report, http://dx.doi.org/10.2172/6442256.

Hellouin de Menibus, A., Auzoux, Q., Mongabure, P., Macdonald, V., Le Jolu, T., Besson, J., Crepin, J., 2014. Fracture of zircaloy-4 cladding tubes with or without hydride blisters in uniaxial to plane strain conditions with standard and optimized expansion due to compression tests. Mater. Sci. Eng. A 604, 57–66. http://dx.doi.org/10.1016/j.msea.2014.02.075.

Hellouin De Menibus, A., Sercombe, J., Auzoux, Q., Poussard, C., 2014. Thermomechanical loading applied on the cladding tube during the pellet cladding mechanical interaction phase of a rapid reactivity initiated accident. J. Nucl. Mater. 453, 210–213. http://dx.doi.org/10.1016/J.JNUCMAT.2014.06.046.

Hong, J.D., Park, M., Holston, A.M.A., Stjärnsäter, J., Kook, D., 2021. Threshold stress intensity factor of delayed hydride cracking in irradiated and unirradiated zircaloy-4 cladding. J. Nucl. Mater. 543, 152596. http://dx.doi.org/10.1016/j.jnucmat.2020.152596.

Introïni, C., Ramière, I., Sercombe, J., Michel, B., Helfer, T., Fauque, J., 2024. ALCYONE: the fuel performance code of the PLEIADES platform dedicated to PWR fuel rods behavior. Annals of Nuclear Energy 207, 110711. http://dx.doi.org/10.1016/j.anucene.2024.110711.

Jensen, C., Kamerman, D., Folsom, C., Seo, S., 2023. HERA M&S Exercise Problem Description Report. Technical Report.

Jernkvist, L.O., Massih, A.R., Rudling, P., 2004. A Strain-based Clad Failure Criterion for Reactivity Initiated Accidents in Light Water Reactors. Technical Report, https://www.stralsakerhetsmyndigheten.se/en/publications/reports/safety-at-nuclear-power-plants/2004/200432/.

Kamerman, D., Bachhav, M., Yao, T., Pu, X., Burns, J., 2023. Formation and characterization of hydride rim structures in zircaloy-4 nuclear fuel cladding tubes. J. Nucl. Mater. 586, 154675. http://dx.doi.org/10.1016/J.JNUCMAT.2023.154675.

Kearns, J.J., 1967. Terminal solubility and partitioning of hydrogen in the alpha phase of zirconium, zircaloy-2 and zircaloy-4. J. Nucl. Mater. 22, 292–303. http://dx.doi.org/10.1016/0022-3115(67)90047-5.

Lacroix, E., Motta, A.T., Almer, J.D., 2018. Experimental determination of zirconium hydride precipitation and dissolution in zirconium alloy. J. Nucl. Mater. 509, 162–167. http://dx.doi.org/10.1016/j.jnucmat.2018.06.038.

Lassmann, K., Hohlefeld, F., 1987. The revised URGAP model to describe the gap conductance between fuel and cladding. Nucl. Eng. Des. 103, 215–221. http://dx.doi.org/10.1016/0029-5493(87)90275-5.

Le Saux, M., Besson, J., Carassou, S., 2015. A model to describe the mechanical behavior and the ductile failure of hydrided zircaloy-4 fuel claddings between 25 °c and 480 °c. J. Nucl. Mater. 466, 43–55. http://dx.doi.org/10.1016/j.jnucmat.2015.07.026.

Le Saux, M., Besson, J., Carassou, S., Poussard, C., Averty, X., 2009. Behavior and failure of uniformly hydrided zircaloy-4 fuel claddings between 25 °c and 480 °c under various stress states, including RIA loading conditions. Eng. Fail. Anal. 17, 683–700. http://dx.doi.org/10.1016/j.engfailanal.2009.07.001.

Maki, H., Ooyama, M., 1975. Plastic deformation and fracture behavior of zircaloy-2 fuel cladding tubes under biaxial stress. J. Nucl. Sci. Technol. 12, 423–435. http://dx.doi.org/10.1080/18811248.1975.9733131.

Moal, A., Georgenthum, V., Marchand, O., 2014. SCANAIR: A transient fuel performance code: Part one: General modelling description. Nucl. Eng. Des. 280, 150–171. http://dx.doi.org/10.1016/j.nucengdes.2014.03.055.

Nagase, F., Fuketa, T., 2005. Investigation of hydride rim effect on failure of zircaloy-4 cladding with tube burst test. J. Nucl. Sci. Technol. 42, 58–65. http://dx.doi.org/10.1080/18811248.2005.9726364.

Nantes, K.R., Jin, M., Motta, A.T., 2024. Modeling hydrogen localization in zircaloy cladding subjected to temperature gradients. J. Nucl. Mater. 589, http://dx.doi.org/10.1016/j.jnucmat.2023.154853.

NEA - Working Group on Fuel Satefy, 2022a. State-of-the-art Report on Nuclear Fuel Behaviour Under Reactivity-initiated Accident Conditions (RIA SOAR). https://www.oecd-nea.org/jcms/pl_74371/state-of-the-art-report-on-nuclear-fuel-behaviour-under-reactivity-initiated-accident-conditions-riasoar.

NEA - Working Group on Fuel Satefy, 2022b. Reactivity initiated accident benchmark phase iii report. https://www.oecd-nea.org/jcms/pl_74391/reactivity-initiated-accident-benchmark-phase-iii-report.

NEA CIP, 2024. Cabri international project. https://www.oecd-nea.org/jcms/pl_24821/cabri-international-project-cip.

NEA FIDES, 2024. Second framework for irradiation experiments (FIDES-II). https://www.oecd-nea.org/jcms/pl_70867/second-framework-for-irradiation-experiments-fides-ii.

NEA HERA, 2024. High burnup experiments in reactivity initiated accident. https://www.oecd-nea.org/jcms/pl_70362/high-burnup-experiments-in-reactivity-initiated-accident-hera-fides-ii-joint-experimental-programme-jeep.

Papin, J., Cazalis, B., Frizonnet, J.M., Desquines, J., Lemoine, F., Georgenthum, V., Lamare, F., Petit, M., 2007. Summary and interpretation of the CABRI REP-na program. Nucl. Technol. 157, 230–250. http://dx.doi.org/10.13182/NT07-A3815.

Rashid, J.Y.R., Montgomery, R.O., Lyon, W.F., 2001. A cladding failure model for fuel rods subjected to operational and accident transients. In: Nuclear fuel behaviour modelling at high burnup and its experimental support Proceedings of a Technical Committee meeting held in Windermere, United Kingdom, 19–23 June 2000. pp. 193–199.

Reymond, M., Sercombe, J., Scolaro, A., 2024. A damage model to describe fuel fragmentation and predict fission gas release during reactivity initiated accident. In: Proceedings of the SMIRT-27 conference, Yokohama, Japan.

Salvo, M., Sercombe, J., Helfer, T., Sornay, P., Désoyer, T., 2015a. Experimental characterization and modeling of UO2 grain boundary cracking at high temperatures and high strain rates. J. Nucl. Mater. 460, 184–199. http://dx.doi.org/10.1016/j.jnucmat.2015.02.018.

Salvo, M., Sercombe, J., Ménard, J.C., Julien, J., Helfer, T., Désoyer, T., 2015b. Experimental characterization and modelling of UO2 behavior at high temperatures and high strain rates. J. Nucl. Mater. 456, 54–67. http://dx.doi.org/10.1016/j.jnucmat.2014.09.024.

Scolaro, Alessandro, 2021. Development of a Novel Finite Volume Methodology for Multi-Dimensional Fuel Performance Applications (Ph.D. thesis). Ecole Polytechnique Fédérale de Lausanne, http://dx.doi.org/10.5075/EPFL-THESIS-8822.

Scolaro, A., Clifford, I., Fiorina, C., Pautz, A., 2020. The OFFBEAT multi-dimensional fuel behavior solver. Nucl. Eng. Des. 358, 110416. http://dx.doi.org/10.1016/j.nucengdes.2019.110416.

Scolaro, A., Fiorina, C., Clifford, I., Brunetto, E., Pautz, A., 2022a. Pre-release validation database for the multi-dimensional fuel performance code OFFBEAT. In: Proceedings of the International Conference on Physics of Reactors, PHYSOR 2022. pp. 2940–2949. http://dx.doi.org/10.13182/PHYSOR22-37789.

Scolaro, A., Fiorina, C., Clifford, I., Pautz, A., 2022b. Development of a semi-implicit contact methodology for finite volume stress solvers. International Journal for Numerical Methods in Engineering 123 (2), 309–338. http://dx.doi.org/10.1002/NME.6857.

Seo, S., Folsom, C., Jensen, C., Kamerman, D., Giaccardi, L., Cherubini, M., Suk, P., Ševeček, M., Sercombe, J., Guénot-Delahaie, I., Scolaro, A., Reymond, M., Kulacsy, K., Herranz, L., Feria, F., Aragón, P., Khvostov, G., Khan, I., Deo, A.K., Rao, R.S., Calabrese, R., Boldt, F., Sappl, J., Falk, F., Arkoma, A., Vincent, G., Tasaki, Y., Kakiuchi, K., Udagawa, Y., Delipei, G., Cheron, C., Corson, J., Zhang, J., Drieu, T., Klouzal, J., Dostal, M., Matocha, V., Kinkorová, T., Fiorina, C., International Fuel Performance Study of Fresh Fuel Experiments for PCMI Effects During Ria Experiments, preprint, https://papers.ssrn.com/abstract=4883226.

Sercombe, J., Aubrun, I., Nonon, C., 2012. Power ramped cladding stresses and strains in 3D simulations with burnup-dependent pellet-clad friction. Nucl. Eng. Des. 242, 164–181. http://dx.doi.org/10.1016/j.nucengdes.2011.08.069.

Sercombe, J., Helfer, T., Federici, E., Leboulch, D., Le Jolu, T., Hellouin de Ménibus, A., Bernaudat, C., 2016. 2D simulation of hydride blister cracking during a RIA transient with the fuel code ALCYONE. EPJ Nucl. Sci. Technol. 2, 22. http://dx.doi.org/10.1051/EPJN/2016016.

Sercombe, J., Masson, R., Helfer, T., 2013. Stress concentration during pellet cladding interaction: Comparison of closed-form solutions with 2d(r,$\theta$) finite element simulations. Nucl. Eng. Des. 260, 175–187. http://dx.doi.org/10.1016/J.NUCENGDES.2013.03.019.

Sercombe, J., Michel, B., Riglet-Martial, C., Fandeur, O., 2020. Modeling of pellet cladding interaction. In: Comprehensive Nuclear Materials, Second Edition. Elsevier, pp. 417–465. http://dx.doi.org/10.1016/B978-0-12-803581-8.00715-3.

Tomiyasu, K., Sugiyama, T., Fuketa, T., 2007. Influence of cladding-peripheral hydride on mechanical fuel failure under reactivity-initiated accident conditions. J. Nucl. Sci. Technol. 44, 733–742. http://dx.doi.org/10.1080/18811248.2007.9711862.

Udagawa, Y., Mihara, T., Sugiyama, T., Suzuki, M., Amaya, M., 2014. Simulation of the fracture behavior of zircaloy-4 cladding under reactivity-initiated accident conditions with a damage mechanics model combined with fuel performance codes FEMAXI-7 and RANNS. J. Nucl. Sci. Technol. 51, 208–219. http://dx.doi.org/10.1080/00223131.2013.859106.

Zullo, G., Pizzocri, D., Scolaro, A., Van Uffelen, P., Feria, F., Herranz, L.E., Luzzi, L., 2024. Integral-scale validation of the sciantix code for light water reactor fuel rods. http://dx.doi.org/10.2139/SSRN.4743656, preprint, https://papers.ssrn.com/abstract=4743656.